Alma Mater Studiorum - Università di Bologna

SCHOOL OF SCIENCE

Department of Chemistry "Giacomo Ciamician"

Master Degree in

Chemistry - Curriculum – "Erasmus Mundus Master in Chemical Innovation and Regulation"

Class LM-54 – Chemical Science

"Structure, Dynamics, and Substituent Effects of Sulfa-Drugs and their Model Compounds by Free Jet Rotational Spectroscopy and Model Calculations"

CANDIDATE

Maybel Nonato

SUPERVISOR

Prof. Sonia Melandri

CO-SUPERVISOR

Prof. Assimo Maris

Session II

Academic Year 2014-2015

Summary

Sulfa-drug derivatives (Figure 1), such as Benzenesulfonamide (BSA), *para*-Toluenesulfonamide (*p*-TSA), *ortho*-Toluenesulfonamide (*o*-TSA), and Sulfanilamide (SAM), are a group of polar organic compounds which have widespread applications in the chemical industry. However, sulfa-drug derivatives are touted as emerging environmental pollutants. Unfortunately, there is scarcity with regards to their eco-toxicological data but some insights can be gained by analysing their molecular structure and conformational properties which can help us understand also their biological mechanisms and their reactivity.

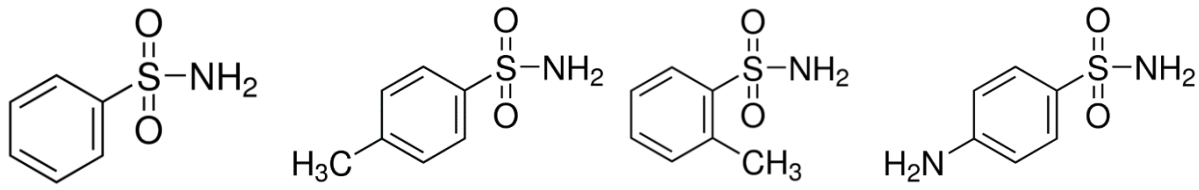

BSA **p-TSA** **o-TSA** **SAM**

Figure 1 - Molecular structure of sulfa-drugs analysed within the study

These information can be obtained from rotational spectroscopy. It is a high resolution tool for the investigation of spatial arrangement of atoms and dynamical properties of molecules in the static gas phase or with supersonic jet techniques. Line spectra in the microwave region usually arise from the transitions between rotational states of gas molecules and the measured frequency of these spectral lines have great accuracy. If the energy of the stationary states can be determined from these measurements, and if expressions for the energy in terms of physical parameters (bond lengths, bond angles, and atomic masses) can be derived, then a precise determination of these parameters can be made. Hence, the data that will be obtained are vital for the understanding of molecular recognition which characterizes various biological mechanisms. Moreover, the experimental data are supported by high level theoretical calculations to which they can be directly compared since they are obtained in the same isolated conditions.

Regarding sulfa-drug derivatives, V. Petrov *et al.* [1-2] conducted a combined study of Gas Electron Diffraction (GED) and quantum chemical calculations for BSA (via B3LYP/6-311+G(2df,p) and MP2/6-31G(2fp,p) level), *p*-TSA (via B3LYP/6-311+G** and MP2/6-31G** level), and *o*-TSA (via B3LYP/6-311+G** and MP2/6-31G** level) while a combined matrix isolation Fourier Transform Infrared Spectroscopy (FTIR) and theoretical DFT (B3LYP)/6-311++G(3df,3pd) was performed on SAM by A. Borba *et al* [3]. Thus, the following results were found: (a) BSA has a symmetry plane (C_s point group) with the S-N bond perpendicular to the benzene ring and the $–NH_2$ group staggering or eclipsing the $–SO_2$ group with the latter as the global minimum; (b) *p*-TSA also has two stable conformers similar to BSA with the eclipsed orientation as the most favoured form; (c) *o*-TSA can have a planar orientation with the S-N bond pointing away from the methyl group or non-planar conformation with the S-N bond perpendicular to the benzene ring. In both cases, the sulfonamide amino group can either adopt a staggered or eclipsed orientation; and (d) SAM has four conformers which vary depending on the orientation of the sulfonamide moiety (either in eclipsed or staggered position) and H atoms of the *p*-amino group (pointing away or directed towards the methyl ring).

The previous studies performed on the four sulfa-drug compounds are quite extensive but the structural information coming from the GED experiment is only an average overall of the vibrational states that are populated at the temperature of the measurement while FTIR can only reach an accuracy close to fractions of cm^{-1}. Hence, these two techniques are not as accurate as rotational spectroscopy which, on the other hand, can provide very precise structural data on different molecular conformations because it probes the rotational transitions exactly at the lowest vibrational ground state.

In this dissertation, the four sulfa-drug derivatives were analysed using rotational free jet spectroscopy coupled with a higher level quantum chemical calculations (B3LYP /6-311++G** and MP2/6-311++G**), with respect to previous studies [1-3], to obtain their structural information and conformational properties. The effect of the added substituents (*ortho*/*para*-CH_3 and *para*-NH_2), in terms of structural parameters, were investigated as well since BSA is the molecular backbone of *o*-TSA, *p*-TSA, and SAM.

Benzenesulfonamide (BSA)

Theoretical calculations for BSA (Table 1) showed the presence of two stable conformers where the S-N bond is perpendicular to the benzene ring and the $-NH_2$ group either staggers or eclipses the $-SO_2$ group with the latter as

the global minimum (BSA_1). This could be explained by electrostatic interaction between the O and H atoms of the sulfonamide group, where opposite charges attract. In contrast, the staggered conformation is less favourable because of the strong repulsion between the nitrogen and oxygen lone pairs.

Table 1 – Molecular geometry and spectroscopic parameters of the stable BSA conformers obtained using B3LYP and MP2 at 6-311++G** level of theory.

	BSA_1		**BSA_2**	
	B3LYP	**MP2**	**B3LYP**	**MP2**
A	2571	2572	2574	2575
B	822	832	820	830
C	718	725	716	722
μ_a	2.61	2.42	4.82	-4.76
μ_b	0.00	0.00	0.00	0.00
μ_c	-3.01	-2.94	-3.72	-3.62
ΔE	0.00[a]	0.00[b]	2.75	1.24
ΔE_0	0.00[c]	0.00[d]	3.56	5.00
I/I_0[e]	1.00	1.00	0.48	0.29
	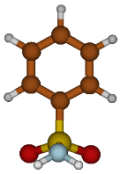		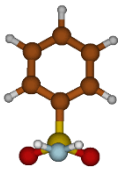	

[a] Absolute energy = -836.327623599 hartree; **[b]** Absolute energy = -834.5833582168 hartree; **[c]** Absolute energy = -836.200943 hartree; **[d]** Absolute energy = -834.457246 hartree; **[e]** Based on the zero point corrected relative energies with the consideration of the square of dipole moment ratio.

Only the eclipsed form was found which was confirmed by recording the spectrum of the deuterated species. On the other hand, the presence of the staggered conformer in the spectrum was anticipated because its predicted relative intensity should be sufficient for detection. However, we were not able to detect the staggered conformer due to conformational relaxation taking place inside the supersonic-jet expansion or the energy of the conformer is higher than the calculated value. Moreover, no splitting due to any internal rotation was observed because of the high S-N rotational energy barrier (20.08 kJ/mol via MP2 and 18.83 kJ/mol via B3LYP) theoretically calculated by V. Petrov *et al* [1]. A structural refinement of the ab initio structure of BSA_1 was also performed to better reproduce the observed rotational constants obtaining a partial experimental structure.

***para*-Toluenesulfonamide (*p*-TSA)**

Quantum chemical calculations for *p*-TSA (Table 2) predicted four stable conformers possessing C_s symmetry which differ for the orientation of the sulfonamide moiety or methyl group in *para* position. The *trans*-eclipsed form (PTS_1) was found to be the global minimum, stabilized by the effects mentioned above and the electronic effects exerted by the methyl substituent.

Table 2 - Molecular geometry and spectroscopic parameters of the stable p-TSA conformers obtained using B3LYP and MP2 methods at 6-311++G** level of theory.

	PTS_1		**PTS_2**		**PTS_3**		**PTS_4**	
	B3LYP	**MP2**	**B3LYP**	**MP2**	**B3LYP**	**MP2**	**B3LYP**	**MP2**
A	2539	2538	2540	2540	2539	2538	2538	2537
B	554	560	553	558	553	558	554	560
C	505	509	504	508	504	508	505	509
μ_a	-3.27	-3.01	-5.54	-5.40	-5.55	-5.41	3.28	-3.01
μ_b	0.00	0.00	0.00	0.01	0.00	0.00	0.00	0.00
μ_c	-2.95	-2.87	-3.63	-3.45	-3.70	-3.50	3.02	-2.94
ΔE	0.00**[a]**	0.00**[b]**	2.69	0.79	2.71	0.83	0.55	0.03
ΔE_0	0.00**[c]**	0.00**[d]**	3.50	2.57	3.53	2.65	0.32	0.09
I/I_0[e]	1.00	1.00	0.55	0.68	0.56	0.69	0.96	1.02

	PTS_1		PTS_2		PTS_3		PTS_4	
	B3LYP	**MP2**	**B3LYP**	**MP2**	**B3LYP**	**MP2**	**B3LYP**	**MP2**
	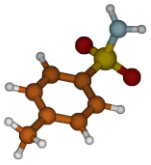		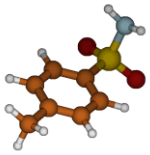		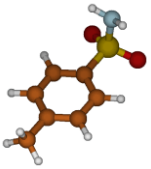		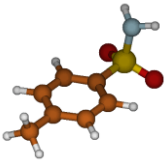	

[a] Absolute energy = -875.656160299 hartree; **[b]** Absolute energy = -873.78424415594 hartree; **[c]** Absolute energy = -875.502398 hartree; **[d]** Absolute energy = -873.629671 hartree; **[e]** Based on the zero point corrected relative energies with the consideration of the square of dipole moment ratio.

Only PTS_1 and PTS_2 were anticipated to be observed in the spectrum, despite the high predicted relative intensity of all four. It is expected that the conformers differing for the position of the methyl group (PTS_1/PTS_4 and PTS_2/PTS_3) will relax to the lower of the two conformations because of the low energy barrier to the methyl rotation. However, three species were found which were hypothesized related to the observation of another conformer or related to a state generated by a large amplitude motions. Unfortunately, we were not able to determine which among the four predicted conformers were found in the spectrum. This problem can be solved by deuteration which was not performed due to the weak intensities of the lines, low sensitivity of the spectrometer, and time limits. Lastly, we can say that from our theoretical calculations, the addition of a weak electron donor methyl group in the *para* position has no significant effects on the structural parameters with respect to BSA (see Table 3).

Table 3 – Selected geometric parameters of BSA, *p*-TSA, *o*-TSA, and SAM from MP2/6-311G++** calculation.

Parameter	BSA	*p*-TSA	*o*-TSA	SAM
S7-C1	1.77698 Å	1.77398 Å	1.78151 Å	1.76761
N8-S7	1.67926 Å	1.6802 Å	1.68386 Å	1.68320
O11-S7	1.45376 Å	1.4541 Å	1.45489 Å	1.45553
O12-S7			1.45397 Å	1.45442
<H9-N8-S7	110.338º	110.194º	110.151º	110.551
<H10-N8-S7			105.553º	109.020
<O11-S7-C1	107.616º	107.649 º	107.516º	107.446
<O12-S7-C1			109.427º	108.480

***ortho*-Toluenesulfonamide (*o*-TSA)**

Differently from the previous case, four plausible conformers were found in the ab initio characterization of *o*-TSA (Table 4) either having a planar configuration with the S-N bond pointed away from the methyl group or a non planar form with the S-N bond perpendicular to the benzene ring. In both cases, the amino group can either adopt a staggered or eclipsed form with respect to the $-SO_2$ group. Hence, the non-planar eclipsed form (OTS_1) was the most stable conformer due to the attractive interaction between the oxygen atom and aromatic C-H group.

Table 4 - Molecular geometry and spectroscopic parameters of the stable *o*-TSA conformers obtained using B3LYP and MP2 methods at 6-311++G** level of theory.

	OTS_1		OTS_2		OTS_3		OTS_4	
	B3LYP	**MP2**	**B3LYP**	**MP2**	**B3LYP**	**MP2**	**B3LYP**	**MP2**
A	1727	1730	1722	1723	1729	1734	1735	1738
B	812	822	807	818	809	818	805	813
C	628	634	624	630	626	631	624	629
μ_a	2.47	2.30	4.54	4.51	-2.09	-1.88	-3.82	-3.80
μ_b	1.25	0.95	1.64	1.2	2.65	2.54	3.44	3.30
μ_c	-2.91	-2.86	-3.40	-3.28	0.02	0.70	0.02	0.66
ΔE	0.00[a]	0.00[b]	6.80	5.46	5.14	5.42	13.62	12.46
ΔE_0	0.00[c]	0.00[d]	6.96	6.70	4.39	5.80	12.49	12.82
I/I_0[e]	1.00	1.00	0.18	0.19	0.00	0.01	0.00	0.00

	OTS_1		OTS_2		OTS_3		OTS_4	
	B3LYP	**MP2**	**B3LYP**	**MP2**	**B3LYP**	**MP2**	**B3LYP**	**MP2**
	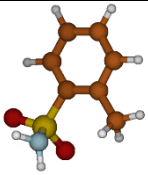		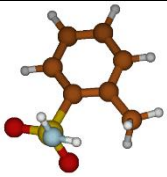		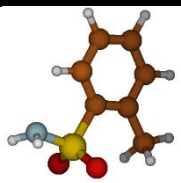		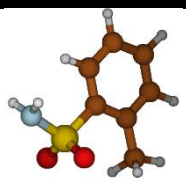	

[a] Absolute energy = -875.651508439 hartree; **[b]** Absolute energy = -873.78231822576 hartree; **[c]** Absolute energy = -875.496991 hartree; **[d]** Absolute energy = -873.626894 hartree; **[e]** Based on the zero point corrected relative energies with the consideration of the square of dipole moment ratio.

Only the rotational spectrum belonging to the global minimum (OTS_1) was observed, which was expected because of the low predicted relative intensities of the other three conformers and the overall intensity of the spectrum. All the rotational transitions showed a splitting due to internal methyl rotation. The V_3 energy barrier (6.081(5) kJ/mol) is comparable to V. Petrov *et al.*'s [2] theoretical one (5.858 kJ/mol via B3LYP/6-311+G**). This shows that the energy barrier of *o*-TSA is much higher compared to the barrier for internal rotation in *p*-TSA (0.126 kJ/mol via B3LYP/6-311+G**) which is also calculated by V. Petrov *et al* [2]. This can be a proof of the interaction between the methyl and sulfonamide group in which rotation is hindered in *o*-TSA unlike in *p*-TSA where there is almost free methyl rotation. Lastly, addition of methyl group in the *ortho* position of BSA brought some dramatic changes in terms of bond angles which clearly shows that the preference for the structure of the global minimum is due to attractive interaction between the oxygen atom and aromatic C-H group (see Table 3 for comparison of selected structural parameters).

Sulfanilamide (SAM)

SAM has four theoretically predicted conformers (Table 5) which differ for the orientation of the sulfonamide moiety or amino group in the *para* position. Wherein, the global minimum (SAM_1) exists in an eclipsed arrangement of the $-SO_2$ and with the H atoms of the *p*-amino group pointed away on the other side of the phenyl ring. Preference for this form is due to the formation of anti-parallel bond dipole interaction.

Table 5 - Molecular geometry and spectroscopic parameters of the stable SAM conformers obtained using B3LYP and MP2 methods at 6-311++G** level of theory.

	SAM_1		SAM_2		SAM_3		SAM_4	
	B3LYP	**MP2**	**B3LYP**	**MP2**	**B3LYP**	**MP2**	**B3LYP**	**MP2**
A	2540	2556	2555	2557	2554	2556	2555	2557
B	556	561	555	560	556	561	555	560
C	506	510	505	508	506	510	505	508
μ_a	-4.73	-4.09	-7.00	-6.41	-4.68	-3.96	-6.99	-6.36
μ_b	-0.05	0.09	-0.00	-0.00	0.00	0.05	0.00	-0.00
μ_c	-2.15	-1.89	-2.85	-2.45	-3.76	-3.94	-4.45	-4.52
ΔE	0.00[a]	0.00[b]	2.26	0.31	0.29	0.35	2.98	1.12
ΔE_0	0.00[c]	0.00[d]	3.30	1.64	0.12	-0.28	3.77	2.59
I/I_0[e]	1.00	1.00	0.67	1.04	2.95	4.73	1.43	2.68
	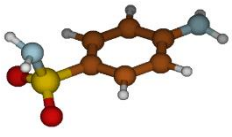		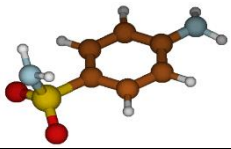		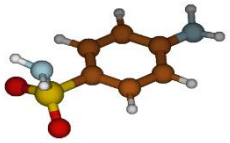		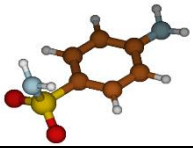	

[a] Absolute energy = -891.707242153 hartree; **[b]** Absolute energy = -889.81685340541 hartree; **[c]** Absolute energy = -891.564105 hartree; **[d]** Absolute energy = -889.672869 hartree; **[e]** Based on the zero point corrected relative energies with the consideration of the square of dipole moment ratio

According to A. Borba *et al.* [3], SAM has a high energy barrier associated with the internal rotation around the N-C bond of *p*-amino group (30 kJ/mol) and low energy barriers associated with internal rotation around the S-C bond (10 to 15 kJ/mol, which vary depending on the orientation of the *p*-amino group); inversion of N atom of *p*-amino group (1.5 kJ/mol); internal rotation around N-S bond (14 kJ/mol); and inversion of N atom of the sulfonamide group (6 kJ/mol). These data allowed A. Borba *et al.* [3] to conclude that the higher energy conformers

will undergo conformational relaxation to the most stable form (SAM_1), which was eventually confirmed via FTIR experiment. Surprisingly different from BSA, the optimized structure of SAM (via B3LYP/6-311++G** and MP2/6-311++G**) is not symmetric. The unusual conformation was verified by launching a surface calculation and frequency calculation with constrained symmetry. However, the results clash with each other as the frequency calculation showed that the asymmetric form is the minimum while surface calculation says otherwise. Hence, it would be very interesting to perform rotational spectroscopy experiment on SAM in the hope of better describing its effective structure and strange behaviour. Moreover, if He will be used as a carrier gas, conformational relaxation might be prevented. Thus, there is a possibility to observe SAM_2 in the spectrum. Lastly, there was no significant structural differences, with respect to BSA, when the *p*-amino group was introduced even though it is a strong electron donor (see Table 3 for comparison of selected structural parameters).

References

[1] V. Petrov, V. Petrova, G.V. Girichev, H. Oberhammer, N.I. Giricheva, & S. Ivanov. (2006). Molecular Structure and Conformations of Benzenesulfonamide: Gas Electron Diffraction and Quantum Chemical calculations. *J. Org. Che. 71*, 2952-2956

[2] V.M. Petrov, G.V. Girichev, H. Oberhammer, V.N. Petrova, N.I. Giricheva, A.V. Bardina, & S.N. Ivanov. (2008). Molecular Structure and Conformations of *para*-Methlybenzene Sulfonamide and *ortho*-Methylbenzene Sulfonamide: Gas Electron Diffraction and Quantum Chemical Calculations Study. *J. Phys. Chem., 112*, 2969-2976. doi: http://dx.doi.org/10.1021/jp710532z

[3] A. Borba, A. Gomez-Zavaglia, & R. Fausto. (2013). Conformational Landscape, Photochemistry, and Infrared Spectra of Sulfanilamide. *J. Phys. Chem. 117*, 704-717. doi: http://dx.doi.org/10.1021/jp311789fl

Declaration of Authorship and Copyright

I hereby declare that I am the author of this work, which is original and unpublished. Authors and works consulted are properly cited in the text and listed in the list of references included.

Maybel Nonato

Acknowledgement

I would like to express my deepest gratitude to the following:

To Professor Sonia Melandri, my thesis supervisor, for her scientific support, guidance, and research ideas.

To Dr. Assimo Maris for patiently teaching and helping me perform my theoretical calculations and molecular modelling.

To Dr. Camilla Calabrese and Dr. Annalisa Vigorito for all their kindness and technical assistance.

To my family, friends, and EMMC-ChIR classmates for their invaluable support and encouragement

Lastly, to the European Commission for the scholarship funded within the Erasmus+ KA1 Programme, ref. 2013-0241 – Erasmus Mundus Joint Master Degree in Chemical Innovation and Regulation.

Abstract

Sulfa-drug derivatives, such as Benzenesulfonamide (BSA), *para*-Toluenesulfonamide (*p*-TSA), *ortho*-Toluenesulfonamide (*o*-TSA), and Sulfanilamide (SAM), are widely used in the chemical industry. However, these polar organic compounds constitute emerging environmental concerns. Unfortunately, there is lack of eco-toxicological data for these substances but some insight can be obtained by analyzing the molecular structure and conformational properties of the compounds which can aid with the understanding of their biological mechanisms. Rotational spectroscopy coupled with high level theoretical calculations can supply these data. In this dissertation, the structural information and conformational properties of the sulfa-drug derivatives were obtained by a combined study of rotational spectroscopy in free jet expansions and quantum chemical calculations (B3LYP and MP2 at 6-311++G** level of theory). The effect of the added substituents (*ortho*/*para*-CH_3 and *para*-NH_2), in terms of structural parameters, were investigated as well since BSA is the molecular backbone of *o*-TSA, *p*-TSA, and SAM. Results showed that the four sulfa-drug derivatives favour the eclipsed conformation of the $–NH_2$ and $–SO_2$ groups but rationalization behind this preference varies among the compounds. Conversely, addition of $–CH_3$ and $–NH_2$ in the *para* position has no significant effects on the structural parameters of BSA but addition of *ortho*-CH_3 brought some dramatic changes in the bond angles.

Keywords: rotational spectroscopy, sulfonamides, ab initio calculations, conformation analysis

Riassunto

Derivati dei farmaci sulfamidici, come benzensolfonammide (BSA), *para*-Toluensolfonammide (*p*-TSA), *orto*-Toluensolfonammide (*o*-TSA), e Sulfanilammide (SAM), sono ampiamente utilizzati nell'industria chimica. Tuttavia, questi composti organici polari costituiscono una emergente preoccupazione ambientale. Purtroppo, vi è la mancanza di dati ecotossicologici per tali sostanze, ma qualche informazione può essere ottenuta analizzando la struttura molecolare e le proprietà conformazionali dei composti che possono aiutare la comprensione dei meccanismi biologici. La spettroscopia rotazionale accoppiata a calcoli teorici di alto livello è in grado di fornire questi dati. In questa tesi, le informazioni strutturali e le proprietà conformazionali dei derivati de farmaci sulfamidici sono stati ottenuti da uno studio combinato di spettroscopia rotazionale in espansione supersonica e calcoli quantistica a livello (B3LYP e MP2/6-311 ++ G **). L'effetto dei sostituenti (*orto* / *para*-CH3 e para-NH2), è stato studiato in termini di parametri strutturali, in quanto BSA constituice la spina dorsale molecolare di *o*-TSA, *p*-TSA, e SAM. I risultati hanno mostrato che i quattro derivati sulfamidici sono caratterizzati da una conformazione eclissata dei gruppi -NH2 ed -SO2, ma la razionalizzazione di questa preferenza varia da composto a composto. Dai risultati ottenuti risulta che la sostituzione con un gruppo, -CH3 e -NH2 nella posizione para non ha effetti significativi sui parametri strutturali della BSA, ma l'aggiunta di *orto*-CH3 ha comportato alcuni cambiamenti drammatici negli angoli obbligazionari.

Parole chiave: spettroscopia rotazionale, sulfamidici, calcoli ab initio, analisi conformazionale

Table of Contents

List of Tables

List of Figures

Abbreviations

Ar: Argon;

BSA: Benzenesulfonamide;

DFT: Density Functional Theory

FJAMMW: Free Jet Absorption Millimetre-Wave;

FT: Fourier Transform;

FTIR: Fourier Transform Infrared Spectroscopy;

GED: Gas Electron Diffraction;

He: Helium

MW: Microwave;

***o*-TSA:** *ortho*-Toluenesulfonamide;

***p*-TSA:** *para*- Toluenesulfonamide;

SAM: Sulfanilamide

Chapter 1 - Introduction

Sulfa-drugs are a family of polar organic compounds which have widespread applications in the chemical industry. In particular, benzenesulfonamide (BSA) is used as an intermediate for the synthesis of dyes, photochemicals, and disinfectants.[1-2] On the other hand, *para*-toluenesulfonamide (*p*-TSA) is utilized as a plasticizer, an intermediate for pesticide and drugs, and is the primary degradation product of the disinfectant chloramine-T (*N*-sodium-*N*-chloro-*p*-toluenesulfonamides) in water.[1-3] *Ortho*-toluenesulfonamide (*o*-TSA) is employed in the production of saccharin, an artificial sweetener.[1] Lastly, sulfanilamides (SAM) are well-known anti-bacterial[4], anti-cancer[5], anti-inflammatory agent[6], and carbonic anhydrase inhibitors.[7]

There are growing concerns with regards to the eco-toxicity and reactivity of these molecular compounds as they are persistent and non-biodegradable. Thus, sulfa-drugs are considered as emerging pollutants not just in the aquatic system but as well as in the terrestrial environment. Unfortunately, there is scarcity with regards to the eco-toxicological data of these compounds.[8] Nonetheless, this can be obtained through an in-depth analysis of their molecular structure and conformational properties which can yield to the understanding of their biological mechanism and intermolecular interactions.

Rotational spectroscopy is a suitable source for this kind of information. It is a high resolution tool for the investigation of spatial arrangement of atoms and dynamical properties of molecules in the static gas phase or with supersonic jet techniques. The wealth of detailed information that can be obtained from a rotational spectrum is vital for the understanding of molecular recognition which characterizes various biological mechanisms. Consequently, simple theoretical calculations are employed as support of the experimental data.[9]

A combined study of Gas Electron Diffraction (GED) and quantum chemical calculations were reported for BSA[10] (via B3LYP/6-311+G(2df,p) and MP2/6-31G(2fp,p) level), *p*-TSA[11] (via B3LYP/6-311+G** and MP2/6-31G** level), and *o*-TSA[11] (via B3LYP/6-311+G** and MP2/6-31G** level) while a combined matrix isolation Fourier Transform Infrared Spectroscopy (FTIR) and theoretical DFT (B3LYP)/6-311++G(3df,3pd) was conducted on SAM.[12] Thus, the following results were found: (a) BSA has a mirror plane (C_s) symmetry with the S-N bond perpendicular to the benzene ring and the $–NH_2$ group staggering or eclipsing

the $-SO_2$ group with the latter as the global minimum; (b) *p*-TSA also has two stable conformers similar to BSA with the eclipsed orientation as the most favoured form; (c) *o*-TSA can have a planar orientation with the S-N bond pointing away from the methyl group or non-planar conformation with the S-N bond perpendicular to the benzene ring. In both cases, the sulfonamide amino group can either adopt a staggered or eclipsed orientation; and (d) SAM has four conformers which vary depending on the orientation of the sulfonamide moiety (either in eclipsed or staggered position) and H atoms of the *p*-amino group (pointing away or directed towards the phenyl ring).

The previous studies performed on the four sulfa-drug compounds are quite extensive but the structural information coming from the GED experiment is only an average overall of the vibrational states that are populated at the temperature of the measurement[13] while FTIR can only reach an accuracy close to fractions of cm^{-1}. Hence, these two techniques are not as accurate as rotational spectroscopy, which on the other hand, can provide the precise structural data and conformation because it probes the rotational transitions exactly at the lowest vibrational ground state.[14]

In the present study, sulfa-drugs were analysed using rotational free jet spectroscopy coupled with higher level DFT and ab initio calculations, with respect to previous studies[10-12], to highlight the possible conformations of the molecules which can help explain their mechanism of reactivity. Consequently, the effect of the added substituents (*ortho*/*para*-CH_3 and *para*-NH_2), in terms of structural parameters, were investigated as well since BSA is the molecular backbone of *o*-TSA, *p*-TSA, and SAM (which can be seen in Table 1.1). Hence, all information derived from the spectroscopy study will be valuable for the assessment of the behaviour and fate of these organic pollutants as well as for the design and development of sulfa-drugs with better efficacy.

Table 1.1 - Molecular structure of sulfa-drugs analysed within the study

STRUCTURE	NAME
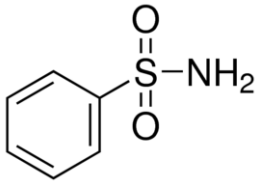	Benzenesulfonamide (BSA)
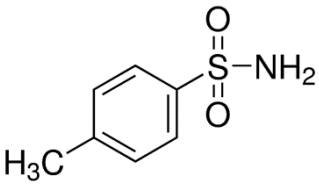	*para*-Toluenesulfonamide (*p*-TSA)
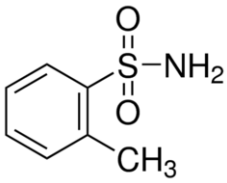	*ortho*-Toluenesulfonamide (*o*-TSA)
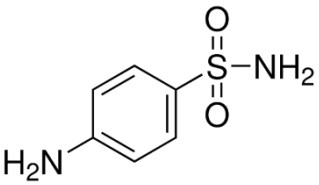	Sulfanilamide (SAM)

Results showed that these four sulfa-drug compounds favour the eclipsed orientation of the -NH_2 and -SO_2 groups. However, rationalization behind this preference varies among the compounds. We might expect that addition of –CH_3 or –NH_2 substituents in the *para* position has no significant effects on the structural parameters of BSA but addition of –CH_3 in the *ortho* position could bring some dramatic changes (in terms of bond angles). In any case, an in-depth discussion of the theoretical and experimental results for these compounds can be found in Chapters 5-8.

Chapter 2 - Fundamental Theory

The microwave (MW) spectra of the molecular compounds studied in this research were interpreted by: (1) describing the rotational level energies of an asymmetric rotor - the theoretical model of the molecular systems being studied in this research; (2) calculating the transition frequencies through the application of section rules; and (3) predicting the appearance of the spectrum by considering the transition moments and population of the states.

This chapter will only provide a brief introduction of the basic concepts utilized within the spectroscopic studies of sulfa-drugs and its model compounds. An extensive list of theories and recent innovations on rotational spectroscopy can be found in various books[15-18] and scientific articles that will be cited when needed.

2.1 Moments of Inertia

Line spectra in the microwave region usually arise from the transitions between rotational states of gas molecules. The measured frequency of these spectral lines have great accuracy. If the energy of the stationary states can be determined from these measurements, and if expressions for the energy in terms of physical parameters (bond lengths, bond angles, and atomic masses) can be derived, then a precise determination of these parameters can be made. This method can obtain values of bond lengths and mass ratios with an accuracy of 1 part in 10^4 or better.

Depending on the configuration of their nuclei, molecules can be classified as linear, spherical tops, symmetric tops (prolate or oblate), or asymmetric tops. The moment of inertia I about any axis is defined by:

$$I = \sum m_i r_i^2 \qquad \textbf{Eqn. 2.1}$$

Wherein, m_i is the mass and r_i is the distance from the axis of the i^{th} nucleus. The locus of the $I^{-1/2}$ plotted along axes passing through the center of gravity and conveniently oriented, is an ellipsoid, called the inertial ellipsoid, whose equation is:

$$I_x x^2 + I_y y^2 + I_z z^2 = 1 \qquad \textbf{Eqn. 2.2}$$

Where I_x, I_y, and I_z are the principal moments of inertia. The inertial ellipsoid is convenient for describing the rotational motion in rigid bodies as it is fixed in the body and rotates with it.

Consequently, molecules can be classified based upon their three principal moments of inertia (presented in Table 2.1).

Table 2.1 - Classification of molecules based upon their moments of inertia.

Type		Molecular Example
Linear	$I_x = 0$; $I_y = I_z$	CO_2; OCS
Spherical Top	$I_x = I_y = I_z$	CH_4
Symmetric Top (Prolate)	$I_x < I_y = I_z$	CH_3Cl
Symmetric Top (Oblate)	$I_x = I_y < I_z$	Benzene
Asymmetric Top	$I_x < I_y < I_z$	Water

The molecules analyzed in the study are asymmetric tops. To be able to understand the rotational properties of asymmetric tops, it is best to relate it with symmetric tops, specifically the energy levels.

2.2 Symmetric Top Molecules

Symmetric top molecules can be classified into either prolate or oblate molecules. The prolate symmetric top molecule is elongated so that its moment of inertia about the symmetry axis is smaller than the two equal moments ($I_x < I_y = I_z$). On the other hand, oblate symmetric top molecule is flattened so that the two equal moments are smaller than the moment about the symmetry axis ($I_x = I_y < I_z$).

According to Classical Mechanics, the total angular momentum $\underset{P}{\rightarrow}$ of a body, in the absence of external forces, has a direction and magnitude fixed in space. However, $\underset{P}{\rightarrow}$ is not fixed in the body. Instead, the top rotates about its symmetry axis with angular momentum $\underset{Pz}{\rightarrow}$, while the symmetry axis precesses with constant angular velocity around the direction of $\underset{P}{\rightarrow}$.

As stated by quantum mechanics, $\underset{P}{\rightarrow}$ is quantized in terms of:

$$|P| = [J(J+1)]^{1/2}\,\frac{h}{2\pi} \qquad \textbf{Eqn. 2.3}$$

Wherein, h is Planck's constant and J is the angular momentum quantum number, taking only integral positive values, starting with zero. Similarly, $\underset{P_z}{\rightarrow}$ can be derived as:

$$P_z = \frac{Kh}{2\pi} \qquad \textbf{Eqn. 2.4}$$

Where, $K = J, J\text{-}1, J\text{-}2, \ldots, -J$

The rotation energy rotation E is defined as:

$$E = \frac{1}{2} I_x \omega_x^2 + \frac{1}{2} I_y \omega_y^2 + \frac{1}{2} I_z \omega_z^2 = \frac{P_x^2}{2I_x} + \frac{P_y^2}{2I_y} + \frac{P_z^2}{2I_z} \qquad \textbf{Eqn. 2.5}$$

Wherein, ω_x is the angular velocity (rad s^{-1}). By convention, the principal moments of inertia of symmetric and asymmetric rotors are labelled as I_A, I_B, and I_C, such that $I_A < I_B < I_C$. If z is the direction of the symmetry axis, and x and y are the directions of two other axes of the inertial ellipsoid, then for an oblate symmetric top:

$$\begin{gathered} I_y < I_z \\ I_x = I_y = I_A = I_B \\ I_z = I_C \end{gathered} \qquad \textbf{Eqn. 2.6}$$

Also,

$$P^2 - P_z^2 = P_x^2 + P_y^2 \qquad \textbf{Eqn. 2.7}$$

Thus for a prolate symmetric top,

$$E = \frac{P^2}{2I_B} + P_z^2 \left\{ \frac{1}{2I_C} - \frac{1}{2I_B} \right\} \qquad \textbf{Eqn. 2.8}$$

So, three rotational constants can be defined as:

$$A = \frac{h}{8\pi^2 I_A} \qquad B = \frac{h}{8\pi^2 I_B} \qquad C = \frac{h}{8\pi^2 I_C} \qquad \textbf{Eqn. 2.9}$$

Then, Eqn 2.8 is solved:

$$E = BJ(J+1) + (C - B)K^2 \quad \text{(for an oblate top)} \qquad \textbf{Eqn. 2.10}$$

$$E = BJ(J+1) + (A - B)K^2 \quad \text{(for a prolate top)} \qquad \textbf{Eqn. 2.11}$$

Where, $J = 0, 1, 2, \ldots$ and $K = 0, \pm 1, \pm 2, \ldots, \pm J$

As can be seen from the equations above, because of the relative values of A, B, and C, the energy increases with K for a prolate top ($A > B$) while it decreases for an oblate top ($B > C$).

Moreover, the energy value is independent of the sign of *K*. So, there will be *J*+1 different values of energy for each value of *J*.

The semi-classical theory can be used to derive the selection rules for allowed transitions between rotational energy levels. As long as a molecule has an electric dipole moment, which can interact with the radiation field, then it can absorb or radiate microwave energy. The dipole moment in symmetric top molecules must be aligned with the symmetry axis so the torque due to the interaction cannot have a component along the symmetry axis and $\underset{Pz}{\rightarrow}$ (or *K*) cannot be changed by a transition. So the interaction with the radiation field can only modify the precessional energy of the molecule. The minimum allowable change in total angular momentum $\underset{P}{\rightarrow}$ corresponds to a change of one unit in the quantum number *J*, so that the selection rules for a transition between rotational energy state becomes:

$$\Delta J = \pm 1 \; ; \; \Delta K = 0 \qquad \textbf{Eqn. 2.12}$$

The frequency *v* observed for a transition from quantum number *J* to *J*+1 is:

$$v = \frac{E_{J+1} + - E_J}{h} = 2B(J+1) \qquad \textbf{Eqn. 2.13}$$

The quantum conditions for a symmetric top can be derived and the wave equation can be written as:

$$H\varphi = E_i \varphi_i \qquad \textbf{Eqn. 2.14}$$

Wherein, *H* is the Hamiltonian operator and E_i and φ_i are the total energy and the wave function of the ith state, respectively. Consequently, the total energy E_i consists of 5 terms:

$$E_i = T + V + U + 0 + R \qquad \textbf{Eqn. 2.15}$$

Where, *T* is the translational kinetic energy; *V* is the internuclear potential energy; *U* is the electronic energy; 0 is the vibrational energy; and *R* is the rotational energy. These variables cannot be separated and the wave equation cannot be solved exactly. However, we can consider as a first approximation that the rotational transitions motion is not affected by the other ones (at least for the lower rotational and vibrational states) thus no interaction terms involving rotation is needed to be written in the Hamiltonian.

The translational energy *T* may be treated separately since it is due to motion of the center of the mass. On the other hand, the average internuclear distances of the ground vibrational state

do not change during the rotational of the molecule (at least for the first approximation) so that *V* and 0 remain constant. Moreover, the electronic wave function does not change significantly as the nuclei rotate because the electronic motion is very fast.

The last approximation is called the Born-Oppenheimer approximation which is only applicable for the lower rotational and vibrational states. Thus, the Hamiltonian operator can be written as sum of separate terms while the wave function is the product of separate terms (which allows the rotational variables to be separated and the rotational wave equation to be written independently). This can be derived in terms of Euler's angles $\emptyset, \theta$, and x which provide the orientation of the body axes relative to those in the fixed coordinate system. The time independent rotational equation in terms of Euler's angles can be written as:

$$\frac{1}{sin\theta}\frac{\partial}{\partial\theta}\left(sin\theta\frac{\partial\varphi}{\partial\theta}\right)+\frac{1}{sin^2\theta}\frac{\partial^2\varphi}{\partial\emptyset^2}+\left(\frac{cos^2\theta}{sin^2\theta}+\frac{C}{B}\right)\frac{\partial^2\varphi}{\partial x^2}-\frac{2cos\theta}{sin^2\theta}\frac{\partial^2\varphi}{\partial x\partial\emptyset}+\frac{E}{hB}\varphi=0 \qquad \textbf{Eqn. 2.16}$$

Wherein, *E* is the energy and φ is the wavefunction. Physically significant solutions are possible only for certain discrete values E_J, with corresponding wave functions φ_J. The variables may be separated and the φ written in the form:

$$\varphi = \theta\ (\theta)\ e^{iM\emptyset}e^{iKx} \qquad \textbf{Eqn. 2.17}$$

Wherein, *M* and *K* must be integers 0, ±1, ±2, for φ to be single valued while $\theta\ (\theta)$ is the power series which must terminate and become just a polynomial in order for the wave function to be normalized.

The expressions for the angular momenta Eqn. 2.3 and Eqn. 2.4 are derived from Eqn. 2.17 to the wave equation. Moreover, quantum numbers *J* and *K*, and a third quantum number *M* appears which represents the component of $\underset{P}{\rightarrow}$ along an arbitrary axis (which is introduced by a magnetic or electric field). On the contrary, the energy levels for different *M* are degenerate in the absence of such field.

2.3 Asymmetric Top Molecules

Asymmetric top molecules do not have an axis of symmetry so the rotation around the total angular momentum $\underset{P}{\rightarrow}$ has no preferred direction. Also, the selection rule $\Delta K = 0$ has no meaning even though $\underset{P}{\rightarrow}$ is quantized and the quantum number *J* is defined. Using the symmetric top wave functions as a basis, the approximate energy levels are derived but it will be very difficult

to determine the exact level since they cannot be represented by an explicit formula similar to the symmetric top ones. Fortunately, microwave spectroscopy has overcome these difficulties of analyzing asymmetric top molecule structures.

Even though quantum number *K* is not significant for the asymmetric top, there are still 2*J*+1 energy levels for each value of *J*, which is similar to the symmetric top. Wherein, the degenerate levels of the symmetric cases are separated while each level of the asymmetric top has a different energy. For slight deviations from the symmetric top, the splitting of the levels is small and the quantum number *K* is approximately defined and the energy levels may be obtained by perturbation methods. Unfortunately, there is no quantum number with any physical meaning to distinguish between the 2*J*+1 levels of equal *J*. The sublevels are labelled simply as:

$$J_\tau \ (\tau = -J, -J+1, -J+2, \ldots +J)$$

In order of increasing energy, the lowest level J_{-J}, the next J_{-J+1}, and so up to J_J. *King, Hainer, and Cross*[20] derived the energy levels which can be expressed as:

$$E = \frac{1}{2}(A + C)J(J+1) + \frac{1}{2}(A - C)E_\tau \qquad \textbf{Eqn. 2.18}$$

Wherein, *A, B, C* are the rotational constants defined in Eqn. 2.9 while E_τ is the numeric reduced energy which is a function of *J* and of an asymmetry parameter κ, defined by Ray[21] as:

$$\kappa = \frac{2B - A - C}{A - C} \qquad \textbf{Eqn. 2.19}$$

For a prolate top, κ = -1 while it will be κ = +1 for an oblate top and values near zero for highly asymmetric top. The parameter κ can be viewed as continuous parameter with all asymmetric tops lying between these two extreme cases. The non-crossing rule is applied to link the energy levels and the two limiting quantum numbers K_a and K_c serve to label each level. The relationship between J_τ and $J_{Ka,Kc}$ system of labels is $\tau = Ka - Kc$. It can be noted that $K_a + K_c = J$ or $J+1$.

The 2*J*+1 values of E_τ for a given *J* are the roots of a secular determinant of degree 2*J*+1, retrieved from the application of group theory to the symmetry properties of the molecule. The determinant can be factorized into a number of determinants of smaller degree, leading to a number of algebraic equations in each case. Some of these equations are listed in various texts.[15-16],[22] However, with increasing *J*, their degrees increases which makes the calculation

of E_τ values extremely difficult. With the advancement in technology, various software are available for the computation of transition energies. An example would be the SPFIT/SPCAT program[23] which was used in the present study.

On the other hand, the components (μ_a, μ_b, and μ_c) of the permanent dipole moment vector ($\underset{\mu}{\rightarrow}$), along the *a*, *b*, and *c* principal molecular axes, are the basis of the selection rules for asymmetric tops. Hence, the selection rules can be divided into three general cases:

(a) *a*-type transitions when $\mu_a \neq 0$; $\Delta K_a = 0$ ($\pm 2, \pm 4, \ldots$); $\Delta Kc = \pm 1$ ($\pm 3, \pm 5, \ldots$)

(b) *b*-type transitions when $\mu_b \neq 0$; $\Delta K_a = \pm 1$ ($\pm 3, \ldots$); $\Delta Kc = \pm 1$ ($\pm 3, \ldots$)

(c) *c*-type transitions when $\mu_c \neq 0$; $\Delta K_a = \pm 1$ ($\pm 3, \pm 5, \ldots$); $\Delta Kc = 0$ ($\pm 2, \pm 4, \ldots$)

It can be noted that the transitions inside the parenthesis are weaker compared to the main transitions. Also, all three types of transitions can be found in the rotational spectrum of a molecule of low symmetry if all of its dipole moments are not equal ($\mu_a \neq \mu_b \neq \mu_c$).

2.4 Centrifugal Distortion

As a first approximation, molecules are considered as rigid rotors. However, a real molecule cannot absolutely be rigid since it is subjected to centrifugal forces. Thus, when a molecule rotates, the centrifugal force tends to distort the molecule (stretching the bonds slightly) and change the moment of inertia, and eventually the rotational spectrum.

If distortion is taken into account then the moment of inertia (values of which are dependent on the rotational states) cannot be considered as constant any longer. Thus, the rotational spectrum cannot be considered like a rigid rotor that is characterized by a sequence of equilibrium moments of inertia. Still, centrifugal distortion constants, even at very low levels and relatively small energies, can be determined with the precise measurements of rotational spectroscopy.

The centrifugal distortion effects only represent a small part of the rotational energies which are accounted for mainly by the rigid rotor term. Hence, the effect can be considered as a perturbation to the rigid rotor Hamiltonian H_R. The total Hamiltonian is represented by the equation:

$$H = H_R + H_D \qquad \textbf{Eqn. 2.20}$$

Wherein, H_D is the contribution of the centrifugal distortion part and is involved in the first order of perturbation treatment in which H_D was averaged over the asymmetric rigid rotor wave functions. While for the second order perturbation treatment, it is possible to transform H_R into an effective form H_{eff} which is diagonal in the vibrational quantum numbers transforming the Hamiltonian terms of the fourth degree in angular momentum $\underset{P}{\rightarrow}$ (quartic centrifugal distortion terms):

$$H_D = \frac{1}{4}\sum_{\alpha,\beta,\gamma,\delta} \tau_{\alpha\beta\gamma\delta} \underset{P}{\rightarrow}_{\alpha} \underset{P}{\rightarrow}_{\beta} \underset{P}{\rightarrow}_{\gamma} \underset{P}{\rightarrow}_{\delta} \qquad \textbf{Eqn. 2.21}$$

Wherein, $\alpha, \beta = x, y,$ and z permute cyclically. For an asymmetric rotor, $\tau_{\alpha\beta\gamma\delta}$ (quartic centrifugal distortion coefficients) can be reduced to five independent constants as discuss in the review paper of *Watson* **[19]** Thus, the *A*- and *S*- reduced forms of H_D is represented by the equation:

$$H_D^{(A)} = -\Delta_P P^4 - \Delta_{JK} P^2 P_z^2 - \Delta_K P_z^4 - \frac{1}{2}[(\delta_J P^2 + \delta_J P_z^2), (P_+^2 + P_-^2)] \qquad \textbf{Eqn. 2.22}$$

$$H_D^{(S)} = -D_J P^4 - D_{JK} P^2 P_z^2 - D_K P_z^4 - d_1 P^2 (P_+^2 + P_-^2) - d_2 (P_+^4 + P_-^4) \qquad \textbf{Eqn. 2.23}$$

Wherein, $P_{\pm} = P_x \pm P_y$ are the angular momentum ladder operators. More details about the reduction of the rotational Hamiltonian can be found in the review paper by *Watson*.**[19]**

2.5 Quadrupole Coupling Effect

Quadrupole coupling interaction occurs when the spin quantum number (*I*) of a nucleus is greater than ½. Wherein, coupling of nuclear spin angular momentum with rotational angular momentum results to rotational energy level splitting. Thus, *2I+1* level are produced when quantum number *J* of a rotational level is greater than *I* while *2J+1* level are generated if *J* is less than *I*. The energies of the sub levels are proportional to the nuclear quadruple moment and as a function of *F* and *J*, where $F = J + I, J + I - 1, \ldots, 0, \ldots |J - I|$. By observing the quadrupole splitting, we can determine the magnitude and orientation of the nuclear quadrupole moment in the molecule. Hence, the selection rule for the rotational transition will be $\Delta J = \pm 1$; $\Delta F = 0, \pm 1$).

In general, the quadrupole coupling tensor is traceless due to the Laplace equation:

$$X_{aa} + X_{bb} + X_{cc} = 0 \qquad \textbf{Eqn. 2.24}$$

Thus, there are only two independent coupling constants (X and η). Wherein:

$$\eta = \frac{Xaa - Xbb}{Xcc} \qquad \textbf{Eqn. 2.25}$$

On the other hand, as *J* increases, the $F \rightarrow F\text{-}1$ components get weaker thus they become undetectable. Consequently, $F \rightarrow F+1$ are the strongest lines but converge in frequency and become unresolvable as *J* increases.

2.6 Theoretical Calculations

Molecular properties of a molecule can now be calculated with the aid of various commercially available computer programs such as GAUSSIAN, SPARTAN, and GAMESS. In the present study, GAUSSIAN 09 program[24] was used to perform theoretical calculations, which were carried out by providing the following input information: (a) method, level, and kind of calculation to be used; (b) total charge and spin multiplicity of the molecules to be considered; and (c) starting geometry (x,y,z coordinates) of each atom in the molecule (or z-internal coordinates matrix).[25]

DFT (B3LYP)[26-27] and ab initio (MP2)[28] methods at the 6-311++G** level of theory were utilized for the calculations. These methods were successfully used in the past for the description of electronic structures of isolated molecules with a good degree of precision (that is very close to the spectroscopy results). Hence, the following information can be derived from the theoretical calculations which are helpful for the search of rotational spectra and conformational assignment: (a) molecular structures; (b) vibrational frequencies; (c) electronic dipole moment components; (d) centrifugal distortion constants; (e) nuclear quadrupole coupling constants; and (f) electronic energy values.

2.7 Internal Motions

The earliest rotational spectroscopy studies of ammonia is concerned about its inversion motion tunnelling. Since then, the tunnelling splitting found in the rotational spectra of many molecular systems were the basis of the characterization of their large amplitude internal motions. Usually, two or more motions can be generated from tunnelling splitting. Typical motions are: (a) internal rotational of symmetric (generally methyl) groups; (b) inversion of amino or imino hydrogens; (c) internal rotation of light asymmetric groups (OH, SH, NH_2); (d) ring puckering of (saturated) four- or (near saturated) five membered rings; and (e) pseudo-rotation. It is also possible to observe large splitting from heavy atoms (or structural groups) if their motions are characterized

by low barrier potential energy surfaces like in many molecular complexes.[29] These potential barriers are assumed to be generated by the interactions of two groups of electrons and nuclei. Generally, quantum chemical calculations can be used to determine the barrier but the computation will be rigorous. Another approach that can be use is to describe the origin of the barrier in terms of the forces behind their intermolecular interactions (such as Van der Waals forces, resonance forces, etc).

Among the four molecules studied in this dissertation, splitting (due to internal rotation around the methyl group) can only be observed in the rotational spectra of *o*-TSA. Wherein, its experimental V_3 energy barrier (around 6.081(5) kJ/mol) was calculated. On the contrary, it is not possible to observe the splitting in BSA and *p*-TSA while rotational spectroscopy experiment is still needed to be performed on SAM. An in depth discussion of the results of the rotational spectroscopy study of the molecules analyzed in this dissertation can be found in Chapter 5-8.

2.8 Evaluation of Molecular Structure

The rotational spectrum yields the rotational constants (*A*, *B*, and *C*). Herewith, we can derive the moments of inertia which contain the structural information of the molecule. However, it is not always possible to obtain all the structural parameters (for the determination of molecular structure) from the rotational constants. Hence, analysis of the rotational spectra of isotopic substituted species is needed.

Consequently, there are three types of structures frequently used for the study of rotational spectroscopy:

(a) r_e – the equilibrium structure for the hypothetical vibrationless state. In general, this is obtained from theoretical optimization and it can be assessed from the experimental rotational constants if the zero point vibrational corrections to the structure are known.

(b) r_0 – the effective structure for the ground vibrational state. This can be obtained from the ground state rotational constants. The moments of inertia of isotopic substituted species can be evaluated through the use of least squares fitting procedure for the determination of the structural parameter of the molecule:

$$I_i = I_i^0 + \sum_j \frac{\Delta I_i}{\Delta p_i} \Delta p_i \qquad \textbf{Eqn. 2.26}$$

Wherein, I_i is the *i*-th experimental moment of inertia; I_i^0 is the *i*-th moment of inertia derived from the initial assumed structure; p_i is the structural parameter for the fitting; and $\frac{\Delta I_i}{\Delta p_i}$ is the changing of I_i^0 with a small change in p_i while the parameters are kept constant. The procedure will be repeated until convergence is achieved.

For large molecule for which not all the isotopic isotopologues can usually be observed from the structure fitting, only partial r_0 structure can be obtained from the evaluation of several bond lengths, valence angles, or dihedral valence angles. The procedure can also be used for non-covalent interaction bonded molecular complexes for the determination of intermolecular bond length and angles while the geometry of molecular moieties is kept constant.

(c) r_s – the substitution structure. This is calculated from the isotopic substitution method using Kraitchmann's equation. Wherein, the position of an atom with respect to the principal axes of the parent molecule can be determined. However, the method is strictly applied to equilibrium moments of inertia I_e. Thus, the molecule is assumed to be rigid so there are no changes in the bond distances and angles during isotopic substitution.

If the mass of the substituted atom is connoted as $m+\Delta m$, with m as the original mass of the atom then the moments of inertia in the principal axis system of the parent molecule can be expressed by the following equations:

$$I'_a = I_a + \mu\,(b^2+c^2) \qquad \textbf{Eqn. 2.27}$$

$$I'_b = I_b + \mu\,(a^2+c^2) \qquad \textbf{Eqn. 2.28}$$

$$I'_c = I_c + \mu\,(a^2+b^2) \qquad \textbf{Eqn. 2.29}$$

In which, I'_a, I'_b, and I'_c are the principal moments of inertia of the isotopically substituted molecule; I_a, I_b, and I_c are the principal moments of inertia of the parent molecule; and μ is the reduced mass for the isotopic substitution:

$$\mu = \frac{M\Delta m}{M+\Delta m} \qquad \textbf{Eqn. 2.30}$$

Wherein, M is the total mass of the molecule.

2.9 Isotopic Effect

Depending on the moment of inertia, the isotopic effect can have an influence on the molecular spectroscopy of the system especially on the rotational transition frequencies. H→D isotopic substitution can cause changes in the molecular geometry of the molecule, particularly with the bond length thus affecting the strength of hydrogen bonding within molecules. This phenomena is called is called Ubbelohde effect where deuteration increases the hydrogen bond length. We can relate the effect to the fact that in the R-D deuterated form, the ν_0 fundamental frequency of a R-H stretching is reduced by a factor of $\approx 1.4 \approx (m_H/m_{D)})^{1/2}$. Hence, the observed molecular changes can be used to identify the structure of the molecule.

Chapter 3 - Spectroscopic Techniques

3.1 Supersonic Free Jet Spectroscopy

Substantial advances have been made in the field of MW spectroscopy since 1980's when the Balle-Flygare type FTMW spectrometer was invented. One of them is the application of supersonic free jet expansions of the sample for rotational spectroscopic experiments. This method has high sensitivity and selectivity making it a powerful analytical technique for an in-depth study of the structural and dynamics of weakly bound molecules in an unperturbed environment.[30-31]

Supersonic free jets allow for strong adiabatic cooling of the rotational and vibrational degrees of freedom which greatly simplifies the rotational spectrum. Increasing the intensity of the low *J* transitions eliminates high *J* transitions along with most vibrational satellites and higher energy conformers making the rotational assignment very straightforward.[29] Thus, the resulting electronic absorption and emission spectra will contain high intensity sharp lines instead of broad bands at very low temperature.[32]

3.2 FJAMMW Spectrometer

Figure 3.1 – FJAMMW spectrometer

Various types of free jet microwave spectrometers have already been developed. One of them is the free jet Stark modulated absorption millimetre-wave spectrometer, originally built by

Brown et al. at Monash University, Australia.[33] An analogous model, working now in the frequency range of 52-74 GHz, was built in University of Bologna, Italy[34] and used in this dissertation to measure all the rotational spectra of the molecules being studied (depicted in Figure 3.1).

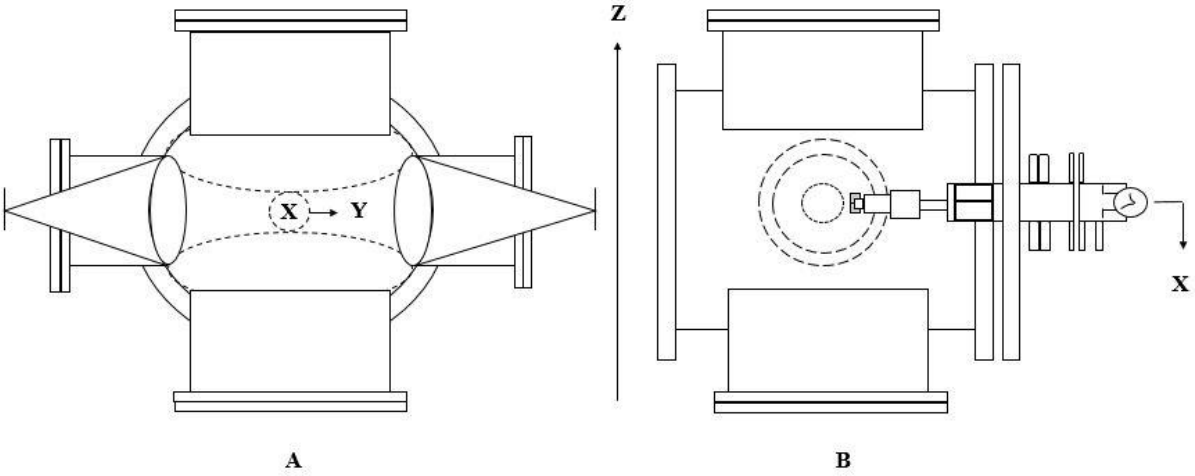

Figure 3.2 – Main components of the FJAMMW spectrometer

The main components of the FJAMMW spectrometer are illustrated in Figure 3.2. The supersonic beam expands along the x-axis (showed in Figure 3.2B) of a cylindrical vacuum chamber 50 cm in diameter and 50 cm in length, which is evacuated with an effective vacuum yield of around 12000 ls^{-1} at about $4x10^{-3}$ mbar.[34]

The nozzles used have a diameter range of 0.02-0.05 cm. They are conveniently small to maintain the characteristics of the vacuum system by increasing the backing (stagnation) pressure P_0 since high pressure is favourable for complex formation. A stainless steel tube connects the nozzle to the outside of the vacuum chamber and is closed by an easily demountable head on which a manometer is mounted for the measurement of the stagnation pressure (Section C). When the tube is open, a sample container (D) made by copper tube of suitable outer diameter and provided with inlet and outlet holes, can be placed in Section B, where the O-ring shown prevents the driving gas from bypassing it. Both the pulsed nozzle and section B of the tube can be heated.[35]

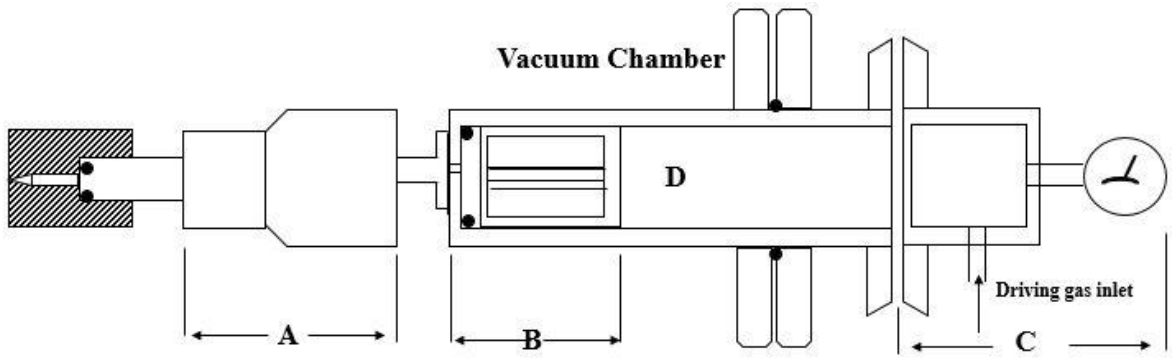

Figure 3.3 – Scheme of the pulsed nozzle

Conversely, the vacuum chamber (see Figure 3.2A) contains four ports through which the microwave radiation interacts with the jet plume. A lens system (Montech-Clayton, Australia) concentrates the radiation into the plume region along the y-axis. There are also two plates (separated around 5cm) that provide the Stark modulation. A voltage of up to 3 kV at a frequency of 33 kHz can be applied to the plates.[34]

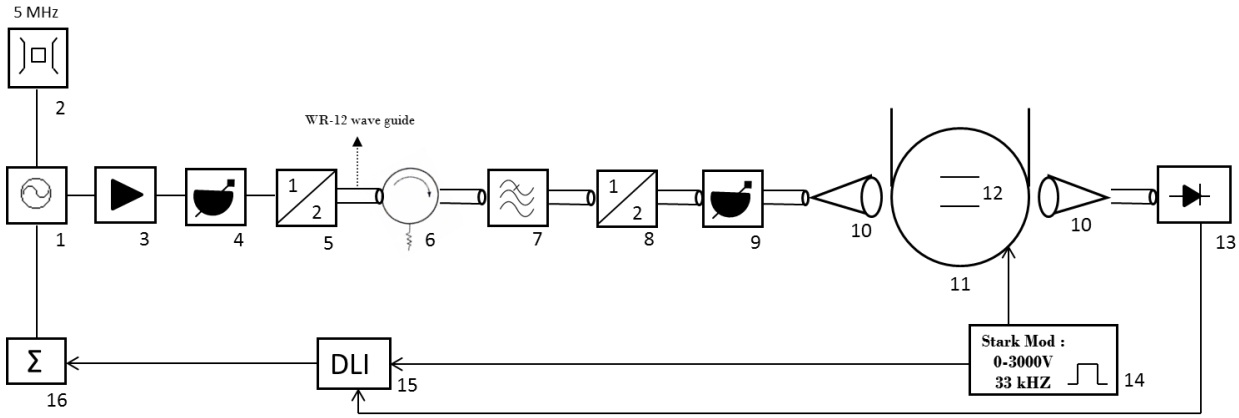

Figure 3.4 - Block diagram of the Free Jet Absorption Millimeter Wave spectrometer (FJAMMW)

The block diagram of the microwave circuit of the FJAMMW spectrometer is illustrated in Figure 3.4. Wherein: Section 1 is the MicroWave synthesizer - HP8672A 2-18GHz is the radiation source; Section 2 is the reference signal, Rb oscillator 5 MHz , Ball-Efraton FRK-LLN which generates the standard frequency to which the synthesizer is locked; Section 3 is the Hittite Amplifier MW 5-20 GHz Gain : +20dB which increases the level of the signal; Section 4 is the variable attenuator, NARDA 10dB which varies the power output to control the input to the amplifier; Section 5 is the frequency doubler Spacek-labs 26.5-40 GHz. Ouput power:

+17dBm; Section 6 is the Dorado Isolator 26.5-40 GHz, 41 GHz; Section 7 is the low pass filter Spacek-labs 41 GHz; Section 8 is the frequency doubler Spacek-labs 53-80 GHz. Ouput power: -3dBm - 0dBm; Section 9 is the variable attenuator 0-35dB; Section 10 is the horn-dielectric lens system (Montech-Clayton, Australia); Section 11 is the supersonic-jet expansion chamber; Section 12 is the stark plates for the Stark effect modulation; Section 13 is the Schottky-diode detector: Millitech DXW10 for frequencies above 60 GHz or a Millitech 4731 4H-1111 for frequencies below 60 GHz; Section 14 is the high voltage Stark modulation: electric field up to 750 V cm^{-1} at a frequency of 33 kHz; Section 15 is the digital lock-in amplifier; and Section 16 is the experimental control and data acquisition system.

Chapter 4 - Methodology

4.1 Theoretical Calculation

Gaussian 09 suite of programs[24] was used to carry out the MP2/6-311++G** and B3LYP/6-311++G** calculations of the molecular structure, conformational energies, electric dipole moment components, and nuclear quadrupole coupling constants on the plausible conformers of BSA, *p*-TSA, *o*-TSA, and SAM. This level of theory was used because it gives results accurate enough to aid the rotational assignment and to guide the identification of the conformers present in the jet expansion.[9] Moreover, it is higher in level with respect to the calculations reported in the previous GED[10-11] and FTIR[12] sulfa-drug derivatives studies.

The calculated vibrational frequencies in the harmonic approximation of all the optimized structures allowed us to verify that the stationary points were the actual minima. Moreover, it allowed us to estimate the zero point vibrational correction to the electronic energy and the values of the quartic centrifugal distortion constants.

Consequently, the ab initio spectroscopic parameters were used to predict the shape of the rotational spectrum with the aid of SPFIT/SPCAT program.[23] The SPCAT program predicts the spectrum with a set of user-defined parameters that are described in two input files (.var and .int file). The parameters are comprised of molecule specific information such as the electric dipole moment in the principal inertia axes system of the molecule, rotational constants, distortion constants, and partition function. These data are the basis of the calculated line positions and strengths. Initial predictions are written in .cat file. Conversely, the SPFIT program utilizes data containing frequency, intensity, and quantum numbers (J, K_a, K_c, v) assigned for transitions to fit such spectroscopic information by a least squares analysis using a user-defined reduction of the Hamiltonian to a user-defined set of rotational and centrifugal distortion constants. A new set of parameters are calculated by the SPFIT program after performing spectral assignment. From this set of parameters, new transitions can be predicted and the process can be reiterated until a satisfactory fit is reached.

A structural refinement of the MP2 (r_e) geometry of the conformers was also performed using the STRFIT (STRucture FITting to rotational data) program[23] to better reproduce the observed

rotational constants obtaining the effective structure (r_0). The program was utilized by fitting the internal coordinates (such as bond lengths, bond angles, and dihedral angles) directly to the moments of inertia in a non-linear least-squares procedure.[36]

4.2 Experimental

Samples of BSA, *p*-TSA, and *o*-TSA were purchased from Alfa Aesar and used without further purification. The compounds were individually analysed using the FJAMMW spectrum in the frequency range of 58.6-74.0 GHz. It is necessary to warm the sample in the carrier gas to obtain a suitable concentration of it (about 4%). The resulting mixture will expand through a nozzle with a diameter of about 0.35 mm. Hence, Table 4.1 summarizes the experimental conditions of each compound to be analysed.

Table 4.1 - Spectroscopic experimental conditions of the molecular samples.

Compound	Purity	Temperature Range (°C)	P_{Ar} (mbar)	P_{He} (mbar)	Stark (V)
BSA	98%	140-150	~200	~500	~3000
p-TSA	99%	130-140	~200	~500	~1000
o-TSA	99%	130-140	~200	-	~3000

P_{Ar} – Pressure using Argon gas
P_{He} – Pressure using Helium gas

The temperature range used is around the melting point of the compound. The sample should be in gas phase and then diluted in the carrier gas because free rotation in liquid or solid phase/s is hindered by intermolecular interactions.

Ar and He were the carrier gas utilized to the dilute the samples in gas phase. They provide a spherical test probe of the electron density and resultant electric fields which influence the van der Waals interaction.[37-38]

Stark effect was employed to improve the signal/noise ratio and the sensitivity of the instrument. This was achieved by allowing an oscillating electric field to act on the sample molecules in which the field creates a periodic oscillating Stark effect that modulates the signal. Thus, the energy levels under investigation are modulated in such a way that the intensity of absorption and observed signals are also modulated.[39]

Before conducting the full spectral analysis, a run test was done to see which experimental conditions work best for the sample molecules (in terms of producing spectra with strong intensities). As can be seen in Table 4.1, only *p*-TSA has a different Stark value. The molecule has a very low intensity and the spectrum produced at ~1000 V has sharper lines than at ~3000 V.

Rotational spectrum of isotopic species is needed to obtain supplemental structural information of the molecular samples. Enriched deuterated species were produced by passing D_2O (99% supplied by Promochem GmbH) in the carrier gas over the heated sample. Thus, the spectroscopic experimental conditions for the generation of various deuterated species can be found in Table 4.2.

Table 4.2 - Experimental conditions for the generation of deuterated species.

Deuterated Specie	Temperature Range (ºC)	Carrier Gas	Pressure (mbar)	Stark (V)
BSA - D_2O	140-150	Ar	~200	~3000
p-TSA - D_2O	-	-	-	-
o-TSA - D_2O	-	-	-	-
NOTE: Deuteration was not performed for other molecular compounds because of the very low intensity already of the normal species, which would prevent the measuring of the spectra of the deuterated ones.				

Chapter 5 - Benzenesulfonamide

5.1 Introduction

The molecular structure and conformational properties of Benzenesulfonamide (BSA) have been reported in the past on the basis of a combined Gas Electron Diffraction (GED) -study and quantum chemical calculations B3LYP/6-311+G(2df,p) and MP2/6-31G(2fp,p) level. According to the GED study[10], BSA belongs to the C_s point group, wherein the only symmetry plane is a mirror plane[39], passing through the S-N bond which is perpendicular to the ring plane. Consequently, the calculations predicted BSA to have a staggered and an eclipsed form with the latter as the global minimum.

Although the study performed by V. Petrov *et. al*.[10] is quite extensive and convincing, the data obtained by GED only represents an average over all vibrational states that are populated at the temperature of the measurement[13], while BSA's precise structural data and conformation can be obtained using rotational spectroscopy which probes the rotational transitions exactly at the lowest vibrational ground state.[14] This should lead to the unequivocal and definite identification of BSA's different conformers and their relative energy scale.

5.2 Theoretical Calculation

In this study, the molecular structure and spectroscopic properties of plausible BSA conformers have been studied by quantum chemical methods (MP2 and B3LYP at 6-311++G** level of theory) and are presented in Table 5.1. The calculations performed were higher in level compared to the theoretical methods used in the GED study of V. Petrov *et. al*.[10] From the calculations we evinced that BSA has two stable conformers where the S-N bond is perpendicular to the benzene ring and the $-NH_2$ group staggering or eclipsing the $-SO_2$ group.

Table 5.1 – Molecular geometry and spectroscopic parameters of the stable BSA conformers obtained using B3LYP and MP2 at 6-311++G** level of theory.

	BSA_1		BSA_2	
	B3LYP	**MP2**	**B3LYP**	**MP2**
Rotational Constants [MHz]				
A	2571	2572	2574	2575
B	822	832	820	830
C	718	725	716	722
Quartic Centrifugal Distortion Constants [kHz]				
D_J	0.04	0.04	0.03	0.03
D_{JK}	0.12	0.25	0.11	0.10
D_K	-0.01	-0.16	0.00	0.00
d_1	-0.00	-0.00	-0.00	-0.00
d_2	0.00	0.01	0.00	0.00
Electric Dipole Moment Components [D]				
μ_a	2.61	2.42	4.82	-4.76
μ_b	0.00	0.00	0.00	0.00
μ_c	-3.01	-2.94	-3.72	-3.62
μ_{tot}	3.99	3.80	6.10	5.93
Nuclear Quadrupole Coupling Constants [MHz]				
χ_{aa}	-2.92	-2.87	-4.97	-4.65
χ_{bb}	1.61	1.56	1.78	1.71
χ_{cc}	1.32	1.31	3.19	2.95
Relative Energies [kJ/mol]				
ΔE	0.00[a]	0.00[b]	2.75	1.24
Zero Point Corrected Relative Energies [kJ/mol]				
ΔE_0	0.00[c]	0.00[d]	3.56	5.00
Relative Intensity of Rotational Transitions[e]				
at T = 150 °C	1.00	1.00	0.48	0.29
Molecular Structure	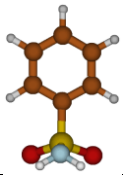		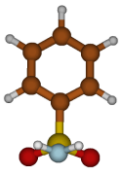	

[a] Absolute energy = -836.327623599 hartree; **[b]** Absolute energy = -834.5833582168 hartree; **[c]** Absolute energy = -836.200943 hartree; **[d]** Absolute energy = -834.457246 hartree; **[e]** Based on the zero point corrected relative energies with the consideration of the square of dipole moment ratio.

According to both DFT (B3LYP) and ab initio (MP2) frequency calculations, the eclipsed conformer (BSA_1) was predicted to possess the minimum. This could be explained by electrostatic interaction between the O and H atoms of the sulfonamide group, where opposite charges attract. In contrast, the staggered conformation is less favourable because of the strong repulsion between the nitrogen and oxygen lone pairs.[10] From the data reported in Table 5.1, it can be seen that it would be quite hard to differentiate the two conformers from their rotational

spectrum since the value of their rotational constants are somewhat similar. We can only discriminate the two conformers through the rotational spectroscopy study of their deuterated species.

5.3 Rotational Spectrum

The rotational constants and values of the dipole moment components found in Table 5.1 were the basis of the preliminary trial calculations of the spectrum of the two conformers of BSA. Hence, the search for the rotational transitions in the frequency range of the spectrometer started using Ar as the carrier gas. Under these conditions, several rotational lines were observed and could be interpreted as originating by a single molecular species, called conformer I. No other signals besides those belonging to conformer I were detected in the spectrum.

Based on the calculated spectra, we expected to see μ_a and μ_c – type transitions but no μ_b transition line/s due to the C_s symmetry of BSA_1 conformer. However, only μ_c – type transitions were observed in the experiment since μ_a-transition lines are supposed to be too weak because of high rotational quantum numbers (J) involved. Spectrum assignment started with the lowest J predicted in the spectral region, in which, $12_{12} \leftarrow 11_{11}$ rotational transition was observed. Afterwards, various spectroscopic assignments were performed up to J = 20, measuring some weaker μ_c transition lines. The S-reduction of Watson's quartic Hamiltonian in the I^r representation[19] was fitted against the experimental frequencies of Table 5.2, giving the spectroscopic constants reported in Table 5.3.

No splitting due to internal rotation was observed in the scanned frequency because of the high S-N rotational barrier energy theoretically calculated at 20.08 and 18.83 kJ/mol by V. Petrov *et al.*[10] using MP2 and B3LYP methods.

To obtain supplemental structural information, the rotational spectrum of the monodeuterated and bideuterated species of BSA, also summarized in Table 5.2, were investigated. Their spectroscopic constants, listed in Table 5.3, were obtained using the same fitting procedure as for the normal species.

The presence of the staggered conformer (BSA_2) in the spectrum was anticipated because its predicted intensity should be sufficient for detection (see Table 5.1). Conformational relaxation

upon supersonic expansion might be the possible reason why the experimental signals for a higher energy specie were not detected in the Ar scan. This process is quite common among conformers that are connected through inter-conversion barriers.[40]

Thus, another scan was performed using He as the carrier gas to prevent conformational relaxation. Under this condition, the measured population ratio in the expansion will be equivalent with the established one at the stagnation temperature and should therefore depend on the relative energy of the conformers and on the temperature before expansion.[41] Unfortunately, only the spectrum of conformer I was observed in the second scan. There are two hypotheses about why the staggered conformer was not detected: (1) its energy is higher than the value suggested by the theoretical calculation or (2) the transition barrier between the two conformations is very low that it relaxes inside the supersonic-jet expansion. The hypotheses can be checked through the theoretical calculation of relative energies and zero point corrected relative energies of the two conformers. However, the results of B3LYP and MP2 methods were inconsistent with one another. It is quite uncertain which method provided the correct data but an error always occur when MP2 calculation is being performed and the cause of the problem is still unknown. Hence, the calculated result of the MP2 method might not be so accurate.

Table 5.2 - Experimental frequencies (ν/MHz) and discrepancies between experimental and calculated values ($\Delta\nu$/MHz) of the measured transitions of the normal, monodeuterated, and bideuterated species of BSA (conformer I).

J'	K'a	K'c	J"	K"a	K"c	I		MONODEUTERATED		BIDEUTERATED	
						ν	$\Delta\nu$	ν	$\Delta\nu$	ν	$\Delta\nu$
14	14	1	13	13	1	71730.50	0.08	70364.62	0.07	69110.53	0.02
14	14	0	13	13	0	71730.50	0.08	70364.62	0.07	69110.53	0.02
14	13	2	13	12	2			66762.04	-0.05	65582.22	-0.09
14	13	1	13	12	1			66762.04	-0.05	65582.22	-0.09
15	15	1	14	14	1					74172.65	-0.09
15	15	0	14	14	0					74172.65	-0.09
15	14	2	14	13	2	73300.54	0.02	71916.50	-0.06	70644.56	0.00
15	14	1	14	13	1	73300.54	0.02	71916.50	-0.06	70644.56	0.00
13	13	0	12	12	0	66475.37	-0.03	65209.97	-0.08		
13	13	1	12	12	1	66475.37	-0.03	65209.97	-0.08		
13	12	2	12	11	2			61607.61	0.03	60520.07	0.07
13	12	1	12	11	1			61607.61	0.03	60520.07	0.07
15	13	3	14	12	3	69615.55	-0.04	68314.12	0.06	67116.38	0.06
15	13	2	14	12	2	69615.55	-0.04	68314.12	0.06	67116.38	0.06

J'	K'a	K'c	J"	K"a	K"c	I		MONODEUTERATED		BIDEUTERATED	
						ν	Δ*ν*	*ν*	Δ*ν*	*ν*	Δ*ν*
16	14	3	15	13	3					72178.60	0.05
16	14	2	15	13	2					72178.60	0.05
16	13	4	15	12	4	71185.46	-0.07	69865.97	0.06	68650.27	0.04
16	13	3	15	12	3	71185.46	-0.07	69865.97	0.06	68650.27	0.04
17	13	5	16	12	5	72755.21	-0.10	71417.60	-0.01		
17	13	4	16	12	4	72755.21	-0.10	71417.60	-0.01		
18	13	6	17	12	6	74324.82	-0.05	72969.19	0.08		
18	13	5	17	12	5	74324.82	-0.05	72969.19	0.08		
12	12	1	11	11	1	61220.38	0.03	60055.53	0.02		
12	12	0	11	11	0	61220.38	0.03	60055.53	0.02		
14	12	3	13	11	3	64360.46	-0.11	63159.47	-0.09	62054.10	0.06
14	12	2	13	11	3	64360.46	-0.11	63159.47	-0.09	62054.10	0.06
15	12	4	14	11	4	65930.57	0.06	64711.50	0.08	63587.91	-0.04
15	12	3	14	11	3	65930.57	0.06	64711.50	0.08	63587.91	-0.04
16	12	5	15	11	5	67500.17	-0.08	66263.10	0.01	65121.71	0.02
16	12	4	15	11	4	67500.17	-0.08	66263.10	0.01	65121.71	0.02
17	12	6	16	11	6	69069.75	0.01	67814.43	-0.10	66655.28	0.06
17	12	5	16	11	5	69069.75	0.01	67814.43	-0.10	66655.28	0.06
18	12	7	17	11	7	70638.96	0.05	69365.59	-0.07		
18	12	6	17	11	6	70638.96	0.05	69365.59	-0.07		
19	12	8	18	11	8	72207.75	0.07	70916.42	0.01		
19	12	7	18	11	7	72207.75	0.07	70916.42	0.01		
20	12	9	19	11	9	73776.04	0.07	72466.68	-0.03		
20	12	8	19	11	8	73776.04	0.07	72466.68	-0.03		
14	11	4	13	10	4	60675.40	-0.01				
14	11	3	13	10	3	60675.40	-0.01				
15	11	5	14	10	5	62245.05	-0.05	61108.45	-0.03	60059.30	0.00
15	11	4	14	10	4	62245.05	-0.05	61108.45	-0.03	60059.30	0.00
16	11	6	15	10	6	63814.48	0.00	62659.92	0.10	61592.72	-0.02
16	11	5	15	10	5	63814.48	0.00	62659.92	0.10	61592.72	-0.02
17	11	7	16	10	7					63125.82	-0.01
17	11	6	16	10	6					63125.82	-0.01
18	11	8	17	10	8	66951.94	-0.02	65761.33	0.04	64658.38	-0.12
18	11	7	17	10	7	66951.94	-0.02	65761.33	0.04	64658.38	-0.12
19	11	9	18	10	9	68519.95	0.09	67311.30	0.06	66190.62	-0.03
19	11	8	18	10	8	68519.95	0.09	67311.30	0.06	66190.62	-0.03
20	11	10	19	10	10	70087.02	-0.02	68860.60	0.08	67722.17	-0.02
20	11	9	19	10	9	70087.02	-0.02	68860.60	0.08	67722.17	-0.02
21	11	11	20	10	11	71653.27	-0.12	70408.92	-0.10	69253.07	0.05
21	11	10	20	10	10	71653.27	-0.12	70408.92	-0.10	69253.07	0.05
21	10	12	20	9	12			66797.84	0.00		
21	10	11	20	9	11			66797.84	0.00		
22	11	12	21	10	12	73218.66	-0.11	71956.52	-0.11		
22	11	11	21	10	11	73218.66	-0.11	71956.52	-0.11		

J'	K'a	K'c	J"	K"a	K"c	I		MONODEUTERATED		BIDEUTERATED	
						ν	Δ*ν*	*ν*	Δ*ν*	*ν*	Δ*ν*
16	10	7	15	9	7	60127.85	0.08				
16	10	6	15	9	6	60127.85	0.08				
17	10	8	16	9	8	61695.76	-0.10	60605.77	-0.04		
17	10	7	16	9	7	61695.76	-0.10	60605.77	-0.04		
18	10	9	17	9	9	63263.22	0.03	62155.19	-0.05	61126.89	-0.08
18	10	8	17	9	8	63263.22	0.03	62155.19	-0.05	61126.89	-0.08
19	10	10	18	9	10	64829.60	-0.01	63703.83	0.00	62657.91	0.05
19	10	9	18	9	9	64829.60	-0.01	63703.83	0.00	62657.91	0.05
20	10	11	19	9	11	66395.04	0.08			64187.75	-0.08
20	10	10	19	9	10	66395.04	0.08			64187.75	-0.08
22	10	13	21	9	13	69521.71	-0.02	68342.97	0.03		
22	10	12	21	9	12	69521.71	-0.02	68342.97	0.03		
23	10	14	22	9	14	71082.73	-0.02	69886.58	0.07		
23	10	13	22	9	13	71082.73	-0.02	69886.58	0.07		
24	10	15	23	9	15	72641.91	-0.01	71428.42	0.06		
24	10	14	23	9	14	72641.91	-0.01	71428.42	0.07		
25	10	16	24	9	16	74199.02	0.02	72968.29	0.03		
25	10	15	24	9	15	74199.02	0.03	72968.29	0.03		
19	9	11	18	8	11	61134.71	-0.09	60092.25	0.05		
19	9	10	18	8	10	61134.71	-0.09	60092.25	0.05		
20	9	12	19	8	12	62696.91	-0.08	61636.89	0.02	60648.50	0.06
20	9	11	19	8	11	62696.91	-0.07	61636.89	0.03	60648.50	0.07
21	9	13	20	8	13	64257.28	0.03	63179.65	-0.09	62174.13	0.08
21	9	12	20	8	12	64257.28	0.05	63179.65	-0.09	62174.13	0.09
22	9	14	21	8	14	65815.32	0.03	64720.58	0.01		
22	9	13	21	8	13	65815.32	0.05	64720.58	0.03		
23	9	15	22	8	15	67370.74	-0.09	66259.03	-0.04		
23	9	14	22	8	14	67370.74	-0.04	66259.03	0.00		
24	9	16	23	8	16	68923.40	-0.12	67794.82	-0.13		
24	9	15	23	8	15	68923.40	-0.01	67794.82	-0.04		
25	9	17	24	8	17	70472.93	-0.09				
25	9	16	24	8	16	70472.93	0.12				
26	9	18	25	8	18	72018.77	-0.19				
26	9	17	25	8	17	72018.77	0.21				
27	9	19	26	8	19	73560.84	-0.11				
27	9	18	26	8	18	73560.27	0.07				
21	8	14	20	7	14	60540.53	-0.26				
21	8	13	20	7	13	60540.53	0.14				
22	8	15	21	7	15	62090.32	-0.34	61081.13	-0.25	60135.33	-0.23
22	8	14	21	7	14	62090.32	0.44	61081.13	0.38	60135.33	0.28
23	8	16	22	7	16	63636.50	-0.08	62610.91	-0.08	61648.79	-0.10
23	8	15	22	7	15	63635.17	0.08	62609.76	-0.02	61647.96	0.05
24	8	17	23	7	17	65178.16	0.06	64136.53	0.02		
24	8	16	23	7	16	65175.53	0.18	64134.36	0.08		

J'	K'a	K'c	J"	K"a	K"c	I		MONODEUTERATED		BIDEUTERATED	
						ν	Δ*ν*	*ν*	Δ*ν*	*ν*	Δ*ν*
25	8	18	24	7	18	66714.67	-0.11	65657.49	-0.04		
25	8	17	24	7	17	66709.95	0.09	65653.59	0.05		
26	8	19	25	7	19	68246.25	0.03				
26	8	18	25	7	18	68237.71	0.06	67166.67	-0.03		
27	8	20	26	7	20	69772.09	0.01				
27	8	19	26	7	19	69757.64	0.13				
28	8	21	27	7	21	71292.06	-0.06				
28	8	20	27	7	20	71267.96	0.02				
29	8	22	28	7	22	72806.22	-0.04				
23	7	17	22	6	17	59864.95	-0.04				
23	7	16	22	6	16	59835.41	0.06				
24	7	18	23	6	18	61391.71	-0.05				
24	7	17	23	6	17	61342.61	0.11				
25	7	19	24	6	19	62914.05	0.03				
25	7	18	24	6	18	62834.27	-0.04				
26	7	20	25	6	20	64432.71	0.08				
26	7	19	25	6	19	64306.95	0.10				
27	7	21	26	6	21	65949.04	0.06				
27	7	20	26	6	20	65755.25	0.03				
28	7	22	27	6	22	67465.05	-0.01				
28	7	21	27	6	21	67173.44	0.01				
29	7	22	28	6	22	68554.42	-0.07				
31	7	24	30	6	24	71174.29	-0.09				
26	6	21	25	5	21	60801.45	0.08				
26	6	20	25	5	20	59701.96	-0.03				
27	6	22	26	5	22	62398.85	0.00				
27	6	21	26	5	21	60908.14	0.03				
28	6	23	27	5	23	64023.42	-0.12				
28	6	22	27	5	22	62059.01	0.11				
29	6	24	28	5	24	65681.06	-0.07				
29	6	23	28	5	23	63164.84	-0.09				
30	6	24	29	5	24	64244.61	-0.09				
31	6	26	30	5	26	69116.55	0.05				
31	6	25	30	5	25	65323.85	0.07				
27	5	23	26	4	23	60124.28	0.09				
28	5	24	27	4	24	62051.23	0.07				
29	5	25	28	4	25	64031.58	-0.14				
30	5	26	29	4	26	66065.29	-0.02				
31	5	27	30	4	27	68150.23	-0.07				
27	4	24	26	3	24	59939.50	-0.02				
28	4	25	27	3	25	62176.99	0.06				
29	4	26	28	3	26	64446.80	0.14				
27	3	25	26	2	25	61160.13	0.02				
28	3	25	27	2	25	60376.15	0.07				

J'	K'a	K'c	J"	K"a	K"c	I		MONODEUTERATED		BIDEUTERATED	
						ν	Δ*ν*	*ν*	Δ*ν*	*ν*	Δ*ν*
28	3	26	27	2	26	63520.09	-0.08				
29	3	26	28	2	26	63013.64	-0.09				
25	17	8	25	16	10	60768.94	-0.02				
25	17	9	25	16	9	60768.94	-0.02				
24	17	7	24	16	9	60774.71	0.05				
24	17	8	24	16	8	60774.71	0.05				
23	17	6	23	16	8	60779.64	-0.08				
23	17	7	23	16	7	60779.64	-0.08				
22	17	5	22	16	7	60784.21	0.03				
22	17	6	22	16	6	60784.21	0.03				
21	17	4	21	16	6	60788.11	0.01				
21	17	5	21	16	5	60788.11	0.01				
20	17	3	20	16	5	60791.60	0.09				
20	17	4	20	16	4	60791.60	0.09				
19	17	2	19	16	4	60794.60	0.12				
19	17	3	19	16	3	60794.60	0.12				
18	17	1	18	16	3	60797.15	0.12				
18	17	2	18	16	2	60797.15	0.12				
17	17	0	17	16	2	60799.22	0.00				
17	17	1	17	16	1	60799.22	0.00				
27	18	9	27	17	11	64448.94	0.08				
27	18	10	27	17	10	64448.94	0.08				
26	18	8	26	17	10	64454.91	0.02				
26	18	9	26	17	9	64454.91	0.02				
25	18	7	25	17	9	64460.26	-0.03				
25	18	8	25	17	8	64460.26	-0.03				
24	18	6	24	17	8	64465.06	-0.04				
24	18	7	24	17	7	64465.06	-0.04				
23	18	5	23	17	7	64469.31	-0.05				
23	18	6	23	17	6	64469.31	-0.05				
22	18	4	22	17	6	64473.12	-0.01				
22	18	5	22	17	5	64473.12	-0.01				
21	18	3	21	17	5	64476.36	-0.08				
21	18	4	21	17	4	64476.36	-0.08				
20	18	2	20	17	4	64479.29	-0.05				
20	18	3	20	17	3	64479.29	-0.05				
19	18	1	19	17	3	64481.88	0.03				
19	18	2	19	17	2	64481.88	0.03				
18	18	1	18	17	1	64483.95	-0.06				
18	18	0	18	17	2	64483.95	-0.06				
20	4	16	19	1	18	61263.96	-0.02				
21	4	17	20	1	19	64389.24	0.02				
18	5	13	17	2	15	62150.12	-0.03				
19	5	14	18	2	16	63408.29	0.05				

J'	K'a	K'c	J"	K"a	K"c	I		MONODEUTERATED		BIDEUTERATED	
						ν	$\Delta\nu$	ν	$\Delta\nu$	ν	$\Delta\nu$
20	5	15	19	2	17	64798.63	-0.03				
21	5	16	20	2	18	66353.84	0.04				
22	5	17	21	2	19	68104.00	-0.10				

Table 5.3 – Experimental spectroscopic parameters of the normal, monodeuterated and bideuterated species of BSA (conformer I).

	I	MONODEUTERATED	BIDEUTERATED
A (MHz)	2627.6570(1)[a]	2577.4081(8)	2531.2910(7)
B (MHz)	838.2802(5)	826.660(7)	815.30(1)
C (MHz)	730.4877(6)	724.156(8)	717.64(1)
D_J (kHz)	-0.0420(4)	-0.052(2)	[-0.04196][b]
D_{JK} (kHz)	-0.099(2)	[-0.09916][b]	-0.099160410
D_K (kHz)	[0][c]	[0][c]	[0][c]
σ[d] (MHz)	0.068119	0.060052	0.059506
N[e]	120	46	27

[a] - standard error in parentheses in units of the last digit; **[b]** - fixed to the value obtained for normal species; **[c]** – fixed to zero; **[d]** - standard deviation of the fit; and **[e]** - number of transitions in the fit.

5.4 Conformation and Structure

Conformational assignment was done by comparing the theoretical (summarized in Table 5.1) and experimental rotational constants (presented in Table 5.3). The data suggests that the observed conformation is the eclipsed conformer (BSA_1) since it is a global minimum, but we should not base the conformational assignment on this information alone since the rotational constants of the staggered conformer (BSA_2) is not so far away from the experimental values.

Sometimes it is possible to evaluate the dipole moment ratio from intensity measurements thus gaining an independent piece of information to use for the assignment. However, we only have μ_c – type transition present in the spectrum so it is not applicable. Nevertheless, the orientation of the molecule can be determined from the substitution coordinates (r_s)[42] of the hydrogen available upon deuteration of the ammonium hydrogen using Kraitchman's method.[see example: 43] Indeed, the experimental coordinates (r_0) of the hydrogen atoms match the structural model values (r_e) for BSA_1 conformer, and not of those of BSA_2 as shown in Table 5.4.

Table 5.4 – Effective structure for ground vibrational state (r_0), experimental substitution (r_s) and MP2/6-311++G** (r_e) coordinates for the ammonium hydrogen atoms of BSA in the principal axes system of the normal species.

	r_0	r_s		r_e	
		H_A /H_D[b]	H_{DD} /H_D[c]	BSA_1	BSA_2
a (Å)	-2.352(3)[a]	±2.312(1)	±2.369(2)	-2.35	1.66
b (Å)	±0.839(0)	±0.805(3)	±0.836(6)	±0.84	±0.84
c (Å)	-1.738(5)	±1.773(2)	±1.670(3)	-1.76	-1.98

[a] – error expressed in units of the last decimal digit.
[b] – Kraitchman's results for the normal and monodeuterated species.
[c] – Kraitchman's results for the bideuterated and monodeuterated species.

5.5 Structural Fitting

A structural refinement of the MP2 (r_e) geometry of BSA_1 conformer was performed using the STRFIT (STRucture FITting to rotational data) program to better reproduce the observed rotational constants obtaining the effective structure (r_0), shown in Table 5.4. The program was used by fitting the most significant internal coordinates (bond lengths, bond angles, and dihedral angles) directly to the moments of inertia in a non-linear least-squares procedure.[36] For this purpose, four bond lengths (S7-C1, N8-S7, O11-S7, O12-S7) and four valence bond angles (<H9-N8-S7, <H10-N8-S7, <O11-S7-C1, <O12-S7-C1)- were modified. The C_s symmetry of the molecule was maintained so that some bond length and angles were set equal (O11-S7= O12-S7; <H9-N8-S7= <H10-N8-S7; <O11-S7-C1= <O12-S7-C1) reducing the number of variables to three bond lengths and two valence angles. The rotational constants produced from the fitting have an accuracy that falls within units of megahertz. Hence, the effective structure of BSA_1 is presented in Table 5.5 while Figure 5.1 shows the numbering of BSA atoms.

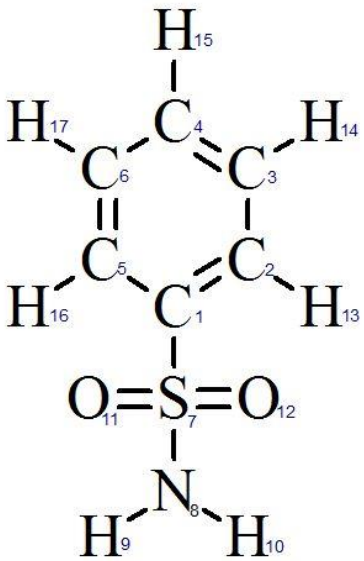

Figure 5.1 - Sketch of BSA showing the number of atoms used in the text.

Table 5.5 - Effective structure calculated from the geometry MP2/6-311++G** of the eclipsed conformer (BSA_1).

Bond Length (Å)		Bond Angle (°)		Dihedral Angle (°)	
C2-C1	1.39829				
C3-C2	1.39856	<C3-C2-C1	118.726		
C4-C3	1.40049	<C4-C3-C2	120.294	<C4-C3-C2-C1	-0.697
C5-C1	1.39829	<C5-C1-C2	121.840	<C5-C1-C2-C3	1.208
C6-C5	1.39856	<C6-C5-C1	118.726	<C6-C5-C1-C2	-1.208
S7-C1	**1.76(8)**[a]	<S7-C1-C2	119.079	<S7-C1-C2-C3	-178.266
N8-S7	**1.66(4)**	<N8-S7-C1	102.418	<N8-S7-C1-C2	89.744
H9-N8	1.01569	**<H9-N8-S7**	**109(7)**	<H9-N8-S7-C1	118.269
H10-N8		**<H10-N8-S7**		<H10-N8-S7-C1	-118.269
O11-S7	**1.42(6)**	**<O11-S7-C1**	**111(9)**	<O11-S7-C1-C5	23.221
O12-S7		**<O12-S7-C1**		<O12-S7-C1-C2	-23.221
H13-C2	1.08571	<H13-C2-C1	119.966	<H13-C2-C1-C5	-178.386
H14-C3	1.08637	<H14-C3-C2	119.638	<H14-C3-C2-C1	-179.691
H15-C4	1.08645	<H15-C4-C3	119.946	<H15-C4-C3-C2	-179.824
H16-C5	1.08571	<H16-C5-C1	119.966	<H16-C5-C1-C2	178.386
H17-C6	1.08637	<H17-C6-C5	119.638	<H17-C6-C5-C1	179.691

[a] - error expressed in units of the last decimal digit. **NOTE:** In bold are the parameters that were modified to produce the experimental values of the rotational constants. The corresponding ab-initio values are: S7-C1 = 1.77698 Å; N8-S7 =1.67926 Å; O11-S7 = 1.45376 Å; O12-S7 = 1.45376 Å; <H9-N8-S7 = 110.338°; <H10-N8-S7 = 110.338°; <O11-S7-C1 = 107.616°; <O12-S7-C1 = 107.616°.

5.6 Conclusion

Information with regards to the conformation, structure, dipole moment, and relative energy of BSA compound was reported. Only the global minimum (eclipsed conformer) was observed experimentally. The conformational preferences could be explained by the electrostatic interaction between the O and H atoms of the sulfonamide group. Failure to observe the staggered conformer is either due to conformational relaxation taking place inside the supersonic-jet expansion or the energy of the conformer is higher than the calculated value. A structural refinement of the ab initio geometry of the BSA_1 conformer (eclipsed form) was also performed to better reproduce the observed rotational constants obtaining a partial experimental structure.

5.7 Recommendation

BSA is known as an emerging pollutant in the aquatic system. Thus, it will be interesting to perform a spectroscopic study on its water complexes to yield an understanding of their mechanism of solvation. For this kind of experiment, it is recommended to use a rotational

spectrometer with a high resolution and sensitivity because the BSA molecule, being a heavy species, shows a very weak intensity of its rotational spectrum even in a free jet spectrometer.

Chapter 6 - *para*-Toluenesulfonamide

6.1 Introduction

It can be noted that *para*-Toluenesulfonamide (*p*-TSA) is a substituted structure of BSA. Introduction of a methyl group in the aromatic ring of BSA may result significant changes not just on the geometric structure but as well as on the physical and chemical properties of the compound. In this work, *p*-TSA was analysed using a combined study of rotational spectroscopy and theoretical calculations (B3LYP and MP2 at 6-311++G** level of theory) to understand the effects of methyl substitution on the structural properties (in terms of bond length, bond angle, and dihedral angle) of BSA.

6.2 Theoretical Calculation

MP2 and B3LYP methods using 6-311++G** basis sets were applied to predict the structure of plausible conformational species of *p*-TSA. Four conformers were found by performing the frequency calculation: (a) *trans*-eclipsed (PTS_1); (b) *trans*-staggered (PTS_2); (c) *cis*-eclipsed (PTS_3); and (d) *cis*-staggered (PTS_4), and their shapes, relative energies, and predicted spectroscopic constants guiding the study are reported in Table 6.1.

Table 6.1 - Molecular geometry and spectroscopic parameters of the stable *p*-TSA conformers obtained using B3LYP and MP2 methods at 6-311++G** level of theory.

	PTS_1		PTS_2		PTS_3		PTS_4	
	B3LYP	**MP2**	**B3LYP**	**MP2**	**B3LYP**	**MP2**	**B3LYP**	**MP2**
Rotational Constants [MHz]								
A	2539	2538	2540	2540	2539	2538	2538	2537
B	554	560	553	558	553	558	554	560
C	505	509	504	508	504	508	505	509
Quartic Centrifugal Distortion Constants [kHz]								
D_J	0.01	0.01	0.01	0.01	0.01	0.01	0.01	0.01
D_{JK}	0.09	0.14	0.08	0.07	0.09	0.07	0.09	0.15
D_K	0.04	-0.01	0.05	0.05	0.05	0.06	0.04	-0.02
Electric Dipole Moment Components [D]								
μ_a	-3.27	-3.01	-5.54	-5.40	-5.55	-5.41	3.28	-3.01
μ_b	0.00	0.00	0.00	0.01	0.00	0.00	0.00	0.00
μ_c	-2.95	-2.87	-3.63	-3.45	-3.70	-3.50	3.02	-2.94
μ_{tot}	4.40	4.16	6.62	6.41	6.67	6.44	4.46	4.21
Nuclear Quadrupole Coupling Constants [MHz]								
χ_{aa}	-2.94	-2.90	-4.98	-4.66	-4.99	-4.67	-2.95	-2.93
χ_{bb}	1.62	1.56	1.78	1.70	1.78	1.70	1.62	1.57
χ_{cc}	1.32	1.34	3.20	2.96	3.21	2.97	1.33	1.37
Relative Energies [kJ/mol]								
ΔE	0.00[a]	0.00[b]	2.69	0.79	2.71	0.83	0.55	0.03

	PTS_1		PTS_2		PTS_3		PTS_4	
	B3LYP	**MP2**	**B3LYP**	**MP2**	**B3LYP**	**MP2**	**B3LYP**	**MP2**
Zero Point Corrected Relative Energies [kJ/mol]								
ΔE_0	0.00[c]	0.00[d]	3.50	2.57	3.53	2.65	0.32	0.09
Relative Intensity of Rotational Transitions[e]								
at T = 140 °C	1.00	1.00	0.55	0.68	0.56	0.69	0.96	1.02
Molecular Structure	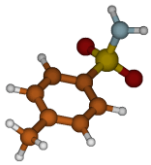		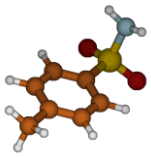		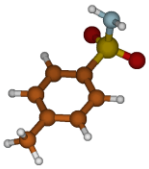		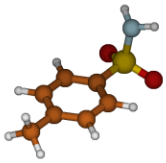	

[a] Absolute energy = -875.656160299 hartree; **[b]** Absolute energy = -873.78424415594 hartree; **[c]** Absolute energy = -875.502398 hartree; **[d]** Absolute energy = -873.629671 hartree; **[e]** Based on the zero point corrected relative energies with the consideration of the square of dipole moment ratio.

The result of the theoretical calculation is quite interesting because only two *p*-TSA conformers, with the $-NH_2$ group either eclipsing or staggering the S-O bonds of the $-SO_2$ group, were previously found using GED and quantum chemical methods (B3LYP/6-311+G** and MP2/6-31G**).[11] Anyhow, the most stable conformer (PTS_1) in the study has the terminal methyl group *trans* with respect to the $-NH_2$ group that is eclipsing the $-SO_2$ moiety. In the trans form, the methyl group minimizes the repulsion with the aromatic hydrogen atoms. The effect of the activating $-CH_3$ group is the destabilization of the staggered form with respect to the eclipsed form (which can be seen at the MP2 calculation of ΔE that goes from 1.24 kJ/mol for BSA to 2.65 kJ/mol for *p*-TSA). Nevertheless, the order of relative energies of the conformers is $E_{PTS1} < E_{PTS4} < E_{PTS2} < E_{PTS3}$.

Consequently, the spectroscopic constants of the four conformers are quite similar to each other which can be seen in Table 6.1. Thus, their differences can only be established through the spectroscopic study of their deuterated species.

6.3 Rotational Spectrum

Preliminary trial calculations of the spectrum were based on the rotational constants found in Table 6.1. The initial search for rotational transitions was performed using Ar as the carrier gas. Under these conditions, a group of rotational lines was observed and interpreted with a set of rotational constants (Conformer I). Afterwards, a second scan was carried out using He as carrier gas (to prevent relaxation) wherein two more sets of transitions were detected and assigned (Conformer II and III). Overall, Conformer I was the most abundant in the spectrum.

Due to the C_s symmetry of *p*-TSA, it is not possible to see μ_b transition line/s. Thus, we only expect the appearance of μ_a and μ_c – type transitions for both conformers. However, the *J* value of μ_a-transition lines is too high for the transitions to be observed in our spectrometer's range. The S-reduction of Watson's quartic Hamiltonian in the I^r representation[19] was fitted against the experimental frequencies of Table 6.2, giving the spectroscopic constants reported in Table 6.3. Lastly, no splitting due to internal rotation around the S-N bond from eclipsed to staggered formation was observed which is in agreement with a high barrier energy for rotation (calculated at 18.284 kJ/mol through B3LYP method by V. Petrov *et. al.*).[11]

Table 6.2 - Experimental frequencies (ν/MHz) and discrepancies between experimental and calculated values ($\Delta\nu$/MHz) of the measured transitions of the three conformer species of *p*-TSA.

						I		II		III	
J'	*K'*a	*K'*c	*J"*	*K"*a	*K"*c	ν	$\Delta\nu$	ν	$\Delta\nu$	ν	$\Delta\nu$
12	12	1	11	11	1	61126.66	-0.06			61119.30	-0.05
12	12	0	11	11	0	61126.66	-0.06			61119.30	-0.05
13	13	1	12	12	1	66395.18	0.10	66475.17	0.02	66383.54	0.03
13	13	0	12	12	0	66395.18	0.10	66475.17	0.02	66383.54	0.03
13	12	2	12	11	2	62203.07	0.11	62283.63	0.10	62195.57	0.05
13	12	1	12	11	1	62203.07	0.11	62283.63	0.10	62195.57	0.05
14	14	1	13	13	1	71663.43	0.05				
14	14	0	13	13	0	71663.43	0.05				
14	13	2	13	12	2	67471.37	0.06	67551.33	0.07	67459.63	0.02
14	13	1	13	12	1	67471.37	0.06	67551.33	0.07	67459.63	0.02
14	12	3	13	11	3	63279.18	-0.01	63359.9	-0.01	63271.60	0.01
14	12	2	13	11	2	63279.18	-0.01	63359.9	-0.01	63271.60	0.01
15	14	2	14	13	2	72739.55	-0.06				
15	14	1	14	13	1	72739.55	-0.06				
15	13	3	14	12	3	68547.60	0.07			68535.56	-0.06
15	13	2	14	12	2	68547.60	0.07			68535.56	-0.06
15	12	4	14	11	4	64355.34	-0.04	64436.06	-0.07		
15	12	3	14	11	3	64355.34	-0.04	64436.06	-0.07		
15	11	5	14	10	5	60163.06	-0.07			60158.51	-0.02
15	11	4	14	10	4	60163.06	-0.07			60158.51	-0.02
16	14	3	15	13	3	73815.78	-0.05				
16	14	2	15	13	2	73815.78	-0.05				
16	13	4	15	12	4	69623.65	-0.08				
16	13	3	15	12	3	69623.65	-0.08				
16	12	5	15	11	5			65512.11	-0.06		
16	12	4	15	11	4			65512.11	-0.06		
16	11	6	15	10	6	61239.15	-0.06			61234.16	-0.02
16	11	5	15	10	5	61239.15	-0.06			61234.16	-0.02

J'	*K*'a	*K*'c	*J*"	*K*"a	*K*"c	I		II		III	
						ν	Δ*ν*	*ν*	Δ*ν*	*ν*	Δ*ν*
17	12	6	16	11	6			66587.95	-0.08		
17	12	5	16	11	5			66587.95	-0.08		
17	11	7	16	10	7	62315.24	0.03	62396.16	-0.03	62309.60	0.02
17	11	6	16	10	6	62315.24	0.03	62396.16	-0.03	62309.60	0.02
18	11	8	17	10	8	63391.12	0.01				
18	11	7	17	10	7	63391.12	0.01				
19	11	9	18	10	9			64547.42	-0.10		
19	11	8	18	10	8			64547.42	-0.10		
19	10	10	18	9	10	60273.64	-0.03			60267.69	0.02
19	10	9	18	9	9	60273.64	-0.03			60267.69	0.02
20	10	11	19	9	11	61348.94	-0.02	61429.45	0.05	61341.28	-0.01
20	10	10	19	9	10	61348.94	-0.02	61429.45	0.05	61341.28	-0.01
21	10	12	20	9	12	62423.92	-0.08	62504.23	0.14	62414.31	0.01
21	10	11	20	9	11	62423.92	-0.08	62504.23	0.14	62414.31	0.01
22	10	13	21	9	13	63498.78	0.01	63578.28	-0.03		
22	10	12	21	9	12	63498.78	0.01	63578.28	-0.03		
23	10	14	22	9	14	64573.22	0.01	64652.14	0.12		
23	10	13	22	9	13	64573.22	0.01	64652.14	0.12		
23	9	15	22	8	15			60453.66	-0.09		
23	9	14	22	8	14			60453.66	-0.09		
24	10	15	23	9	15	65647.33	0.02				
24	10	14	23	9	14	65647.33	0.02				
24	9	16	23	8	16					61424.43	0.00
24	9	15	23	8	15					61424.43	0.00
25	10	16	24	9	16	66720.98	-0.02				
25	10	15	24	9	15	66720.98	-0.02				
26	10	17	25	9	17	67794.22	-0.03				
26	10	16	25	9	16	67794.22	-0.03				
23	9	15	22	8	15	60375.99	0.08				
23	9	14	22	8	14	60375.99	0.08				
24	9	16	23	8	16	61448.84	0.03	61525.58	-0.07		
24	9	15	23	8	15	61448.84	0.03	61525.58	-0.07		
25	9	17	24	8	17	62521.20	0.09	62596.72	0.05		
25	9	16	24	8	16	62521.20	0.09	62596.72	0.05		
26	9	18	25	8	18	63592.72	-0.04				
26	9	17	25	8	17	63592.72	-0.04				
27	9	19	26	8	19	64663.69	0.01				
27	9	18	26	8	18	64663.69	0.01				
27	8	20	26	7	20	60451.70	0.03				
27	8	19	26	7	19	60451.70	0.06				
28	9	20	27	8	20	65733.78	-0.03				
28	9	19	27	8	19	65733.78	-0.03				
28	8	21	27	7	21	61518.16	-0.01				
28	8	20	27	7	20	61518.16	0.06				

J'	*K*'a	*K*'c	*J*"	*K*"a	*K*"c	I		II		III	
						ν	Δ*ν*	*ν*	Δ*ν*	*ν*	Δ*ν*
29	8	22	28	7	22	62583.24	-0.07				
29	8	21	28	7	21	62583.24	0.04				
31	7	25	30	6	25	60448.75	-0.08				
31	7	24	30	6	24	60441.83	0.05				

Table 6.3 – Experimental spectroscopic parameters of the three conformer species of *p*-TSA.

	I	II	III
A (MHz)	2634.33(5)[a]	2639.35(2)	2634.80(1)
B (MHz)	563.12(5)	568.39(1)	575.5(1)
C (MHz)	512.88(1)	510.10(6)	500.3(2)
D_J (kHz)	-0.027(2)	[0][b]	-0.20(2)
D_{JK} (kHz)	[0][b]	-2.81(4)	[0][b]
D_K (kHz)	-0.15(2)	-3.18(8)	-2.92(5)
σ[c] (MHz)	0.054260	0.077021	0.030781
N[d]	34	16	13
[a] - standard error in parentheses in units of the last digit; **[b]** – fixed to zero; **[c]** - standard deviation of the fit; and **[d]** - number of transitions in the fit.			

6.4 Conformation and Structure

Comparing the experimental and theoretical rotational constants, it is quite hard to determine which, among the four plausible conformers, we have observed experimentally since the spectroscopic constants of all species are quite similar with one another. This is probably due to the positioning of the sulfonyl side of the aromatic group and the methyl group. Moreover, the fitting of Conformers II and III are not very accurate because of the difficulty in measuring the transition frequencies due to their very low intensities in the spectrum, which is very near to the sensitivity of the instrument. Thus, assumptions could not be done. In this case, we can only identify the orientation of the molecules through substitution coordinates, available upon its H → D isotopic substitution. However, we did not yet performed deuteration because the detection of deuterated species is limited by the sensitivity of the rotational spectrometer used in the study. Consequently, measurements of the dipole moment ratio which would be very helpful in the assignment - is not applicable since only μ_c – type transition is present in the spectrum.

On the other hand, we only anticipated to observe two conformers in the spectrum instead of three. PTS_1 and PTS_4 belongs to the eclipsed family while PTS_2 and PTS_3 belongs to the staggered family and the positioning of the methyl group is the only difference. Since the energy difference in one family group is very small, it will undergo conformational relaxation in the spectrum. Thus, only two conformers can be seen. There are two hypotheses why three species

were present in the spectrum: (1) another conformer was observed and (2) another state generated by large amplitude motions was detected. We have calculated a barrier energy of 0.598 kJ/mol for internal methyl rotation via B3LYP method which is very low. Probably, the first rotational level is higher and this is the reason why A and E state were not seen in the spectrum. Unfortunately, a technical error always occurs whenever the calculation for the potential surface underlying tunneling effect is launched. The reason behind this is still unknown.

Since deuteration was not performed, structural refinement to better reproduce of the observed rotational constants could not be done. Nevertheless, the internal coordinates (bond lengths, bond angles, and dihedral angles) of the global minimum (PTS_1) are summarized in Table 6.4 while Figure 6.1 shows the numbering of the *p*-TSA atoms. Reactivity of a molecule can be rationalized by its structural parameters.

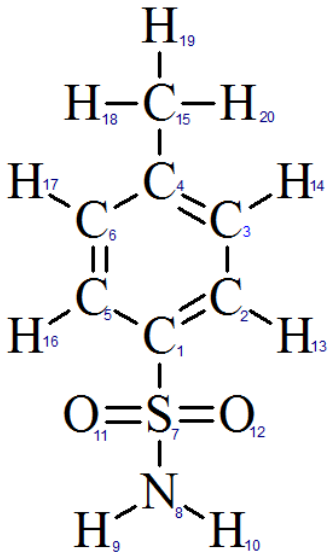

Figure 6.1 - Sketch of *p*-TSA showing the number of atoms used in the text.

Table 6.4 – Structural parameters calculated from the geometry MP2/6-311++G** of the global minima (PTS_1).

Bond Length (Å)		Bond Angle (º)		Dihedral Angle (º)	
C2-C1	1.39771				
C3-C2	1.39765	<C3-C2-C1	118.819		
C4-C3	1.40411	<C4-C3-C2	121.268	<C4-C3-C2-C1	-0.39
C5-C1	1.39771	<C5-C1-C2	121.359	<C5-C1-C2-C3	0.604
C6-C5	1.39765	<C6-C5-C1	118.819	<C6-C5-C1-C2	-0.604
S7-C1	1.77398	<S7-C1-C2	119.313	<S7-C1-C2-C3	-178.015

Bond Length (Å)		Bond Angle (º)		Dihedral Angle (º)	
N8-S7	1.6802	<N8-S7-C1	102.631	<N8-S7-C1-C2	89.324
H9-N8	1.01575	<H9-N8-S7	110.194	<H9-N8-S7-C1	118.444
H10-N8		<H10-N8-S7		<H10-N8-S7-C1	-118.444
O11-S7	1.4541	<O11-S7-C1	107.649	<O11-S7-C1-C5	23.62
O12-S7		<O12-S7-C1		<O12-S7-C1-C2	-23.62
H13-C2	1.0859	<H13-C2-C1	120.039	<H13-C2-C1-C5	-178.901
H14-C3	1.08793	<H14-C3-C2	120.308	<H14-C3-C2-C1	-179.861
C15-C4	1.50837	<C15-C4-C3	120.761	<C15-C4-C3-C2	-178.363
H16-C5	1.0859	<H16-C5-C1	120.039	<H16-C5-C1-C2	178.901
H17-C6	1.08793	<H17-C6-C5	119.308	<H17-C6-C5-C1	179.861
H18-C15	1.09349	<H18-C15-C4	111.02	<H18-C15-C4-C6	30.466
H19-C15	1.09568	<H19-C15-C4	110.735	<H19-C15-C4-C6	-89.256
H20-C15	1.09349	<H20-C15-C4	111.02	<H20-C15-C4-C3	-30.466

NOTE: Numbering of *p*-TSA atoms is illustrated in Figure 6.1.

6.5 Methyl Substituent Effect

Important structural parameters of *p*-TSA and BSA (derived from Table 6.4 and Table 5.5 respectively) are compared in Table 6.5. It can be seen that the introduction of $-CH_3$ group has no appreciable effect on the bond lengths and bond angles of BSA compound since it is a weak electron donor but it is quite interesting that four conformers were produced from it. On the contrary, the influence of $-CH_3$ substituent can also be reflected in the energies of frontier orbitals of the molecule. In a recent study conducted, it was found that introduction of $-CH_3$ group in benzenesulfonic acid slightly increases the HOMO energy of *para*-methylbenzenesulfonic acid.[44] However, it is not possible for us to determine this experimentally since we observe transitions between the rotational energy levels of the molecule in its ground electronic state.

Table 6.5 – Selected geometric parameters of BSA and *p*-TSA from MP2/6-311G++** calculation.

Parameter	BSA[a]	*p*-TSA
S7-C1	1.77698 Å	1.77398 Å
N8-S7	1.67926 Å	1.6802 Å
O11-S7 O12-S7	1.45376 Å	1.4541 Å
<H9-N8-S7 <H10-N8-S7	110.338º	110.194º
<O11-S7-C1 <O12-S7-C1	107.616º	107.649 º

[a] – Original values before structural refinement

6.6 Conclusion

The B3LYP and MP2 calculations predicted four stable conformers possessing C_s symmetry with the *trans*-eclipsed form as the global minimum (PTS_1), stabilized by electronic effects exerted by the methyl substituent. However, analysis of pure rotational spectra of *p*-TSA, recorded in the gas phase under the isolated condition of a supersonic expansion, leads to the observation of three rotational spectra belonging to three different conformers when only two were expected due to conformational relaxation in the spectrum. The hypotheses for this incident are another conformer was observed or it could belong to another state generated by a large amplitude motions. Unfortunately, we were not able to determine which among the four predicted conformers were present in the spectrum since their rotational constants were similar to each other. The conformers can only be differentiated through deuteration which was not performed due to the weak intensities of the conformers and low sensitivity of the machine. Lastly, based on our theoretical calculation, there is only a slight difference between the bond lengths and bond angles of *p*-TSA and BSA since the $-CH_3$ substituent is a weak electron donor.

6.7 Recommendation

H → D isotopic substitution should be performed for conformational identification purposes using a rotational spectrometer with a higher sensitivity and resolution to overcome the weak intensity of the rotational spectra for this species. Structural refinement on the ab initio geometry is also recommended for a better reproduction of the observed rotational constants.

Chapter 7 - *ortho*-Toluenesulfonamide

7.1 Introduction

ortho-Toluenesulfonamide (*o*-TSA) is an analogous structure of *p*-TSA. The only difference between these two BSA substituted compounds is the position where the -CH_3 group is bonded to the ring relative to the -SO_2NH_2 functional group. The position of the added substituent plays a significant role with the conformational preferences of the molecule through the alteration of the geometric and electronic structures. This in turn can change not just the physical and chemical properties of the molecule but also the mechanism of action.

Rotational spectroscopic experiments coupled with theoretical calculations can be used to investigate with a great level of detail the description of the structural and energetic features of the conformational landscape of a molecule. In the previous chapter, it was found that introduction of a weak electron donating –CH_3 substituent in the *para* position of BSA has no appreciable effects on the conformational properties although a different number of conformers was observed for *p*-TSA with respect to BSA. Hence, it will be interesting to study the effects of -CH_3 group in the *ortho* position of BSA for comparison purposes.

7.2 Theoretical Calculation

Full geometry optimization of *o*-TSA has been performed with ab initio (MP2) and DFT (B3LYP) methods using 6-311++G** basis set. Wherein, four plausible conformers were found in the frequency calculation: (a) non-planar eclipsed (OTS_1); (b) non-planar staggered (OTS_2); (c) planar staggered (OTS_3); and (d) planar eclipsed (OTS_4), which is similar to the results of V. Petrov *et. al.*.[11] In our study, the theoretical methods used is higher in level and the respective shapes, relative energy, rotational constants and dipole moment values of the *o*-TSA conformers are presented in Table 7.1.

Table 7.1 - Molecular geometry and spectroscopic parameters of the stable *o*-TSA conformers obtained using B3LYP and MP2 methods at 6-311++G** level of theory.

	OTS_1		**OTS_2**		**OTS_3**		**OTS_4**	
	B3LYP	**MP2**	**B3LYP**	**MP2**	**B3LYP**	**MP2**	**B3LYP**	**MP2**
Rotational Constants [MHz]								
A	1727	1730	1722	1723	1729	1734	1735	1738
B	812	822	807	818	809	818	805	813
C	628	634	624	630	626	631	624	629

	OTS_1		OTS_2		OTS_3		OTS_4	
	B3LYP	**MP2**	**B3LYP**	**MP2**	**B3LYP**	**MP2**	**B3LYP**	**MP2**
Quartic Centrifugal Distortion Constants [kHz]								
D_J	0.02	0.02	0.02	0.02	0.05	0.02	0.04	0.02
D_{JK}	0.05	0.05	0.04	0.05	-0.00	0.05	0.02	0.04
D_K	0.00	0.00	0.01	0.01	0.03	0.01	0.02	0.01
d_1	-0.00	-0.00	-0.00	-0.00	-0.00	-0.00	-0.00	-0.00
d_2	0.00	0.00	0.00	0.00	0.02	0.00	0.01	0.00
Electric Dipole Moment Components [D]								
μ_a	2.47	2.30	4.54	4.51	-2.09	-1.88	-3.82	-3.80
μ_b	1.25	0.95	1.64	1.2	2.65	2.54	3.44	3.30
μ_c	-2.91	-2.86	-3.40	-3.28	0.02	0.70	0.02	0.66
μ_{tot}	4.01	3.78	5.91	5.71	3.37	3.24	5.14	5.07
Nuclear Quadrupole Coupling Constants [MHz]								
χ_{aa}	-2.06	-1.92	-4.88	-4.59	-2.36	-2.13	-4.68	-4.36
χ_{bb}	-0.32	-0.26	1.87	1.75	0.74	0.51	2.72	2.49
χ_{cc}	2.37	2.18	3.01	2.84	1.63	1.62	1.96	1.86
Relative Energies [kJ/mol]								
ΔE	0.00[a]	0.00[b]	6.80	5.46	5.14	5.42	13.62	12.46
Zero Point Corrected Relative Energies [kJ/mol]								
ΔE_0	0.00[c]	0.00[d]	6.96	6.70	4.39	5.80	12.49	12.82
Relative Intensity of the Rotational Transitions[e]								
at T=140 °C	1.00	1.00	0.18	0.19	0.00	0.01	0.00	0.00
Molecular Structure	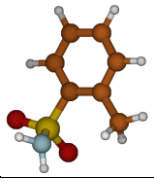		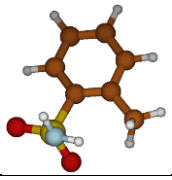		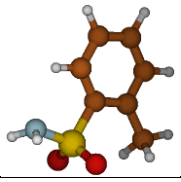		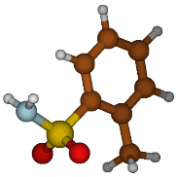	

[a] Absolute energy = -875.651508439 hartree; **[b]** Absolute energy = -873.78231822576 hartree; **[c]** Absolute energy = -875.496991 hartree; **[d]** Absolute energy = -873.626894 hartree; **[e]** Based on the zero point corrected relative energies with the consideration of the square of dipole moment ratio.

As can be seen, OTS_3 and OTS_4 conformers have planar configuration with the S-N bond pointing away from the methyl group while OTS_1 and OTS_2 conformers have non-planar conformation with the S-N bond perpendicular to the benzene ring. In both cases, the amino group can either adopt a staggered or eclipsed orientation with respect to the $-SO_2$ group. The order of relative energies of the conformers is $E_{OTS4} > E_{OTS2} > E_{OTS3} > E_{OTS1}$. Therefore, the OTS_1 conformer will be the most abundant in the jet expansion. Consequently, the detection of higher energy conformers will depend on the overall intensity of the spectrum, and is limited by the sensitivity of the instrument and by relaxation processes.[45] On the other hand, the preference for the non-planar eclipsed conformer can be explained by the attractive interaction between the aromatic C13-H8 group and O12 atom (see Figure 7.1).

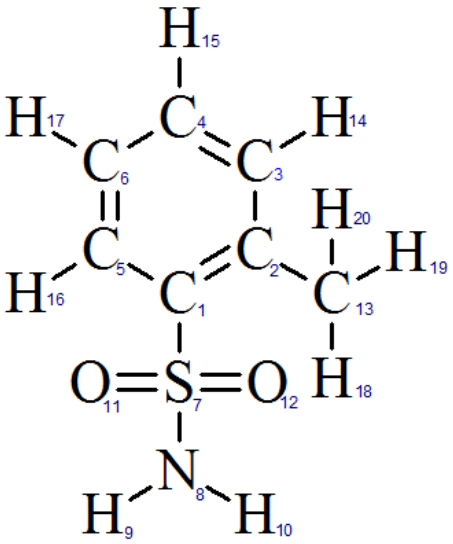

Figure 7.1 - Sketch of *o*-TSA showing the number of atoms used in the text.

7.3 Rotational Spectrum

The rotational spectrum was predicted from the rotational constants of Table 7.1. Under the used experimental conditions (see Chapter 4), the rotational spectrum of conformer I was found. The measured μ_b and μ_c type transitions showed signs of splitting because of internal rotation around the methyl group. No μ_a lines were observed due to weakening of spectral lines at higher J values. Nevertheless, the S-reduction of Wartson's quartic Hamiltonian in the I^r representation[19] was fitted against the experimental frequencies of Table 7.2 using XIAM program (which uses Internal Axis method to treat internal rotation in an asymmetric top molecule)[46], giving the spectroscopic constants reported in Table 7.3. On the other hand, some lines with very weak intensities were remained unassigned in the spectrum.

The search for other *o*-TSA conformers was not performed because the energy barrier between the conformers is high. According to the GED study performed by V. Petrov *et al.*[11], the energy barrier between non-planar and planar conformers is predicted to be 12.13 kJ/mol (B3LYP/6-311+G**) and 13 kJ/mol (MP2/6-31G**). Moreover, the predicted relative intensity for the other three conformers (based on the B3LYP and MP2 methods) and the overall intensity of the spectrum were very low for detection. Thus, only the global minimum (OTS_1) was expected to be seen.

Regarding the methyl group rotation, its theoretical energy barrier of 5.858 kJ/mol (calculated at B3LYP/6-311+G** by V. Petrov *et al.*)[11] can be compared to the V_3 energy barrier (see Table

7.3) of *o*-TSA which is around 6.081(5) kJ/mol, a very high value indeed; much higher than the calculated barrier for *p*-TSA which is 0.126 kJ/mol (calculated at B3LYP/6-311+G** by V. Petrov *et al.*).[11] The large difference in energy barrier values of *o*-TSA and *p*-TSA can be an indication of the interaction between the -CH_3 and -SO_2 group. In *p*-TSA, the methyl group is free to rotate while in *o*-TSA, the methyl group interacts with –SO_2 thus the rotation is hindered and the value of the energy barrier to the rotation of the methyl group is increased.

Table 7.2 – Experimental frequencies (ν/MHz) and discrepancies between experimental and calculated values ($\Delta\nu$/MHz) of the measured transitions of the global minima of *o*-TSA.

J'	*K*'a	*K*'c	*J*"	*K*"a	*K*"c	I	
						ν	$\Delta\nu$
20	20	0	19	19	0	69181.72	-0.10
20	20	0	19	19	0	69181.72	-0.10
20	20	0	19	19	0	69181.72	-0.10
20	20	1	19	19	1	69181.72	-0.10
20	20	0	19	19	0	69182.14	0.02
20	20	0	19	19	0	69182.14	0.02
20	20	0	19	19	0	69182.14	0.02
20	20	1	19	19	1	69181.18	-0.02
20	20	1	19	19	1	69181.18	-0.02
20	20	1	19	19	1	69181.18	-0.02
22	20	2	21	19	2	72127.11	0.06
22	20	3	21	19	3	72127.11	0.06
22	20	3	21	19	3	72126.46	0.04
19	19	0	18	18	0	65672.05	-0.02
19	19	1	18	18	1	65672.05	-0.02
19	19	1	18	18	1	65671.52	0.06
21	19	2	20	18	2	68617.38	0.06
21	19	2	20	18	2	68617.38	0.06
21	19	2	20	18	2	68617.38	0.06
21	19	3	20	18	3	68617.38	0.06
21	19	3	20	18	3	68617.38	0.06
21	19	3	20	18	3	68617.38	0.06
18	18	0	17	17	0	62162.32	0.03
18	18	1	17	17	1	62162.32	0.03
18	18	1	17	17	1	62161.67	-0.01
19	18	1	18	17	1	63635.03	0.03
19	18	2	18	17	2	63635.03	0.03
19	18	2	18	17	2	63634.39	0.00
20	18	2	19	17	2	65107.47	-0.08
20	18	3	19	17	3	65107.47	-0.08
20	18	3	19	17	3	65106.90	-0.04
21	18	3	20	17	3	66579.78	-0.06

J'	*K*'a	*K*'c	*J*"	*K*"a	*K*"c	I	
						v	Δ*v*
21	18	4	20	17	4	66579.78	-0.06
21	18	4	20	17	4	66579.31	0.09
18	17	1	17	16	1	60125.17	-0.01
18	17	2	17	16	2	60125.17	-0.01
18	17	2	17	16	2	60124.55	-0.03
19	17	2	18	16	2	61597.68	-0.04
19	17	3	18	16	3	61597.68	-0.04
19	17	3	18	16	3	61597.14	0.02
20	17	3	19	16	3	63070.00	0.03
20	17	4	19	16	4	63070.00	0.03
20	17	4	19	16	4	63069.39	0.03
21	17	4	20	16	4	64541.81	0.03
21	17	5	20	16	5	64541.81	0.03
21	17	5	20	16	5	64541.28	0.11
22	17	5	21	16	5	66012.96	-0.04
22	17	6	21	16	6	66012.96	-0.04
22	17	6	21	16	6	66012.33	-0.06
20	16	4	19	15	4	61031.70	-0.02
20	16	5	19	15	5	61031.70	-0.02
20	16	5	19	15	5	61031.11	-0.01
22	16	6	21	15	6	63972.82	-0.07
22	16	7	21	15	7	63972.82	-0.07
22	16	7	21	15	7	63972.36	0.08
23	16	7	22	15	7	65441.95	-0.02
23	16	8	22	15	8	65441.95	-0.02
23	16	7	22	15	7	65442.24	-0.03
23	16	8	22	15	8	65441.38	0.03
21	15	6	20	14	6	60462.06	0.01
21	15	7	20	14	7	60462.06	0.01
21	15	6	20	14	6	60462.32	-0.05
21	15	7	20	14	7	60461.41	-0.04
22	15	7	21	14	7	61930.60	0.06
22	15	8	21	14	8	61930.60	0.06
22	15	8	21	14	8	61929.99	0.06
23	15	9	22	14	9	63396.93	0.04
23	14	9	22	13	9	61348.33	0.06
23	14	10	22	13	10	61348.33	0.06
23	14	10	22	13	10	61347.72	0.06
24	14	11	23	13	11	62808.79	-0.04
25	14	12	24	13	12	64267.00	0.01
24	13	11	23	12	11	60746.25	-0.05
24	13	12	23	12	12	60746.25	-0.06
24	13	11	23	12	11	60746.56	-0.06
24	13	12	23	12	12	60745.66	-0.04

J'	*K*'a	*K*'c	*J*"	*K*"a	*K*"c	I	
						ν	Δ*ν*
25	13	12	24	12	12	62197.15	0.09
25	13	13	24	12	13	62197.15	0.07
25	13	13	24	12	13	62196.46	0.01
26	13	13	25	12	13	63642.76	-0.06
26	13	14	25	12	14	63642.76	-0.11
26	13	14	25	12	14	63642.12	-0.11
27	12	15	26	11	15	62960.02	-0.06
27	12	16	26	11	16	62959.41	-0.07
27	11	17	26	10	17	60790.96	0.04
27	11	16	26	10	16	60761.70	0.07
27	11	17	26	10	17	60788.71	0.06
27	11	16	26	10	16	60763.71	0.09
27	11	17	26	10	16	60755.46	-0.05
27	11	16	26	10	17	60797.03	-0.01
27	11	17	26	10	16	60752.31	0.10
27	11	16	26	10	17	60800.18	0.12
28	11	18	27	10	18	62181.63	0.01
28	11	17	27	10	17	62122.42	-0.08
28	11	18	27	10	18	62180.21	0.01
28	11	17	27	10	17	62123.62	-0.02
29	11	19	28	10	19	63564.05	-0.04
29	11	18	28	10	18	63449.59	-0.01
29	11	19	28	10	19	63563.24	-0.06
29	11	18	28	10	18	63450.11	-0.01

Table 7.3 – Experimental spectroscopic parameters of the global minima of *o*-TSA.

	I
A (MHz)	1755.08(1)[a]
B (MHz)	827.06(3)
C (MHz)	637.043(3)
D_{JK} (kHz)	9.6(2)
D_K (kHz)	-0.012(2)
I_α (uÅ^2)	3.202**[b]**
F_0**[c][d]**	157.832
Δ (rad)**[d][e]**	2.02079
V_3 (kJ/mol)	6.081(5)
σ**[f]** (MHz)	0.056109
N**[g]**	68

[a] - standard error in parentheses in units of the last digit; **[b]** – fixed at DFDMS value; **[c]** – $F_0 = 1/I_{\alpha,}$ with I_α as moment of inertia of the top (CH_3); **[d]** – not experimental data but derived from the ab initio MP2 structure; **[e]** – the angle between the internal rotation axis and the principal inertial axis (*a*=*z*) in radiant; **[f]** - standard deviation of the fit; and **[g]** - number of transitions in the fit.

7.4 Conformation and Structure

Comparison of the experimental rotational constants (Table 7.2) with those of the conformational predictions (Table 7.1) shows that OTS_1 is the observed conformer. This can also be proven by the presence of μ_b and μ_c type transitions in the spectrum. Consequently, even though the rotational constants of OTS_3 conformer are not so far away from the experimental values, we are sure that it was not the observed conformer because it should not show any μ_c type lines. H → D isotopic substitution was not performed due to the weak intensity of *o*-TSA conformer. The rotational spectrometer used in the experiment is not suitable for detecting very weak lines because of its low sensitivity.

Alternatively, structural refinement could not be performed since deuteration was not executed. Nevertheless, the structural parameters of the global minimum (OTS_1) are listed in Table 7.4 while Figure 7.1 shows the numbering of the *o*-TSA atoms. Knowledge of the structural parameters of a molecule is important for the rationalization of its reactivity.

Table 7.4 – Structural parameters calculated from the geometry MP2/6-311++G** of the global minima (OTS_1).

Bond Length (Å)		Bond Angle (º)		Dihedral Angle (º)	
C2-C1	1.41060				
C3-C2	1.40355	<C3-C2-C1	116.592		
C4-C3	1.39934	<C4-C3-C2	122.139	<C4-C3-C2-C1	-0.034
C5-C1	1.39993	<C5-C1-C2	122.165	<C5-C1-C2-C3	-0.198
C6-C5	1.39766	<C6-C5-C1	119.614	<C6-C5-C1-C2	0.476
S7-C1	1.78151	<S7-C1-C2	121.221	<S7-C1-C2-C3	179.815
N8-S7	1.68386	<N8-S7-C1	101.484	<N8-S7-C1-C2	67.208
H9-N8	1.01736	<H9-N8-S7	110.151	<H9-N8-S7-C1	96.210
H10-N8	1.01779	<H10-N8-S7	105.553	<H10-N8-S7-C1	-143.305
O11-S7	1.45489	<O11-S7-C1	107.516	<O11-S7-C1-C5	2.264
O12-S7	1.45397	<O12-S7-C1	109.427	<O12-S7-C1-C2	-44.258
C13-C2	2.15812	<C13-C2-C1	123.654	<C13-C2-C1-C5	179.972
H14-C3	1.08770	<H14-C3-C2	118.361	<H14-C3-C2-C1	179.885
H15-C4	1.08663	<H15-C4-C3	119.825	<H15-C4-C3-C2	-179.889
H16-C5	1.08530	<H16-C5-C1	119.243	<H16-C5-C1-C2	179.744
H17-C6	1.08621	<H17-C6-C5	119.798	<H17-C6-C5-C1	179.653
H18-C13	1.09342	<H18-C13-C2	110.877	<H18-C13-C2-C1	-53.742
H19-C13	1.09271	<H19-C13-C2	111.161	<H19-C13-C2-C1	65.849
H20-C13	1.09309	<H20-C13-C2	109.713	<H20-C13-C2-C3	6.572

NOTE: Numbering of *o*-TSA atoms is illustrated in Figure 7.1.

7.5 Methyl Substituent Effect

Table 7.5 shows the comparison of the important structural parameters of BSA, *p*-TSA, and *o*-TSA (retrieved from Table 5.5, Table 6.4, and Table 7.4 respectively). It can be noted that there are no major differences in the bond lengths, from the reference molecule BSA, in spite of the changes in the position of substituent. However, there was a dramatic decrease of <H10-N8-S7 and <N8-S7-C1-C2 and a slight increase of <O12-S7-C1 which clearly shows that the preference of the structure of the global minimum is due to attractive interaction between the aromatic C13-H8 group and O12 atom (see Figure 7.1). This can also be proven by the experimental V_3 energy barrier (see Table 7.3) of *o*-TSA which is around 6.081(5) kJ/mol which is much higher compared with the B3LYP calculated energy barrier for internal rotation in *p*-TSA which is around 0.126 kJ/mol[11]. On the other hand, since the $-CH_3$ substituent is a weak electron donor, the HOMO energy will slightly increase.[47] Since we are observing the transitions between the rotational energy levels of the molecule in its ground electronic state, it is not possible to determine the value of the HOMO energy experimentally.

Table 7.5 – Selected geometric parameters of BSA, *p*-TSA, and *o*-TSA from MP2/6-311G++** calculation.

Parameter	BSA[a]	*p*-TSA	*o*-TSA
S7-C1	1.77698 Å	1.77398 Å	1.78151 Å
N8-S7	1.67926 Å	1.6802 Å	1.68386 Å
O11-S7	1.45376 Å	1.4541 Å	1.45489 Å
O12-S7			1.45397 Å
<H9-N8-S7	110.338°	110.194°	110.151°
<H10-N8-S7			105.553°
<O11-S7-C1	107.616°	107.649 °	107.516°
<O12-S7-C1			109.427°
<N8-S7-C1-C2	89.744°	89.324 °	67.208 °

[a] – Original values before structural refinement

7.6 Conclusion

The rotational spectra of *o*-TSA was investigated using FJAMMW spectrometer. Only the global minimum (non-planar eclipsed conformer) was found which is stabilized by the attractive interaction between the methyl group and O-atom. It is not possible to detect the other conformers due to their low predicted relative intensities and overall intensity of the spectrum. Also, there is a high energy barrier between planar and non planar conformers calculated at 12.13 kJ/mol (B3LYP/6-311+G**) and 13 kJ/mol (MP2/6-31G**) by V. Petrov *et al*.[11] On the other hand, splitting was observed due to the internal rotation around the methyl group. The

experimentally determined barrier is around 6.081(5) kJ/mol which is in good agreement with the calculated B3LYP/6-311+G** barrier by V. Petrov *et al.*[11] around 5.858 kJ/mol. This value of the barrier is much higher that the barrier for internal rotation in *p*-TSA which is around 0.126 kJ/mol (calculated at B3LYP/6-311+G** by V. Petrov *et al.*[11]) and this is an indication of the interaction between the methyl and the amino group. Lastly, the addition of a weak electron donor -CH_3 group in the *ortho* position of BSA has no significant impact on the bond length but it dramatically increases the <H10-N8-S7. It shows that the preference for the structure of the global minimum is due to attractive interaction between the O12 atom and aromatic C-H group.

7.7 Recommendation

A rotational spectrometer with a higher resolution can be used for the detection of the deuterated species of *o*-TSA.

Chapter 8 - Sulfanilamide

8.1 Introduction

Sulfanilamide (SAM) is widely used as an effective chemotherapeutic agent for the prevention and cure of human bacterial infections. Its importance in the pharmaceutical industry led to the study of its molecular geometry and conformation for the determination of its bioactivity, which is the current trend in the drug markets.[12] The resulting information will be beneficial for the design of new effective drugs. In this chapter, we report the results on SAM which was analysed using high level theoretical methods for a more detailed investigation of its structural conformations and electronic properties. Moreover, since SAM is substituted structure of BSA, the effects of the added $–NH_2$ substituent in the *para* position was evaluated.

8.2 Theoretical Calculation

Computational methods (MP2 and B3LYP at 6-311++G** basis set) were used to study the conformational and electronic properties of SAM. The calculations predicted the existence of four conformers which differ for the orientation of the sulfonamide moiety or amino group in the *para* position. Thus, the values of their relative energies, rotational constants, and dipole moments (based on frequency calculation) are reported in Table 8.1.

Table 8.1 - Molecular geometry and spectroscopic parameters of the stable SAM conformers obtained using B3LYP and MP2 methods at 6-311++G** level of theory.

	SAM_1		SAM_2		SAM_3		SAM_4	
	B3LYP	**MP2**	**B3LYP**	**MP2**	**B3LYP**	**MP2**	**B3LYP**	**MP2**
Rotational Constants [MHz]								
A	2540	2556	2555	2557	2554	2556	2555	2557
B	556	561	555	560	556	561	555	560
C	506	510	505	508	506	510	505	508
Quartic Centrifugal Distortion Constants [kHz]								
D_J	0.02	0.01	0.01	0.01	0.03	0.03	0.01	0.01
D_{JK}	0.14	0.11	0.08	0.07	0.23	0.63	0.08	0.07
D_K	0.00	0.03	0.06	0.06	-0.12	-0.52	0.06	0.06
d_1	-0.00	-0.00	-0.00	-0.00	-0.00	-0.00	-0.00	-0.00
d_2	0.01	0.00	0.00	0.00	0.01	0.01	0.00	0.00
Electric Dipole Moment Components [D]								
μ_a	-4.73	-4.09	-7.00	-6.41	-4.68	-3.96	-6.99	-6.36
μ_b	-0.05	0.09	-0.00	-0.00	0.00	0.05	0.00	-0.00
μ_c	-2.15	-1.89	-2.85	-2.45	-3.76	-3.94	-4.45	-4.52
μ_{tot}	5.20	4.51	7.55	6.86	6.00	5.59	8.29	7.80
Nuclear Quadrupole Coupling Constants [MHz]								
χ_{aa1}[a]	2.67	2.54	2.69	2.56	2.54	2.34	2.55	2.35

	SAM_1		SAM_2		SAM_3		SAM_4	
	B3LYP	**MP2**	**B3LYP**	**MP2**	**B3LYP**	**MP2**	**B3LYP**	**MP2**
χ_{bb1}	2.23	1.94	2.22	1.94	2.24	1.95	2.24	1.95
χ_{cc1}	-4.90	-4.48	-4.91	-4.50	-4.77	-4.29	-4.79	-4.30
χ_{aa2}[b]	-2.71	-2.37	-4.97	-4.67	-2.84	-2.70	-4.97	-4.67
χ_{bb2}	1.33	0.73	1.79	1.70	1.62	1.29	1.79	1.71
χ_{cc2}	1.38	1.64	3.19	2.96	1.22	1.42	3.18	2.96
Relative Energies [kJ/mol]								
ΔE	0.00[c]	0.00[d]	2.26	0.31	0.29	0.35	2.98	1.12
Zero Point Corrected Relative Energies [kJ/mol]								
ΔE_0	0.00[e]	0.00[f]	3.30	1.64	0.12	-0.28	3.77	2.59
Relative Intensity of the Rotational Transitions[g]								
at T=140 °C[h]	1.00	1.00	0.67	1.04	2.95	4.73	1.43	2.68
Molecular Structure	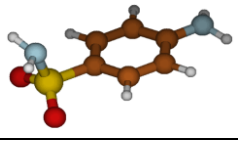		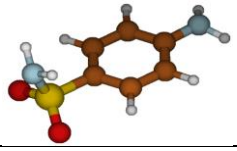		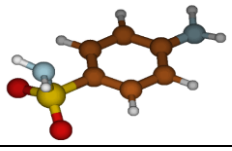		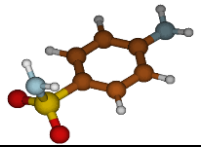	

[a] Refers to N15 (see Figure 8.1); **[b]** Refers to N8 (see Figure 8.1); **[c]** Absolute energy = -891.707242153 hartree; **[d]** Absolute energy = -889.81685340541 hartree; **[e]** Absolute energy = -891.564105 hartree; **[f]** Absolute energy = -889.672869 hartree; **[g]** Based on the zero point corrected relative energies with the consideration of the square of dipole moment ratio; **[h]** Assumed that the experimental temperature will be similar with the previous sulfa-drug compounds.

According to A. Borba *et al.*[12] SAM has five different degrees that can give rise to four different conformers, internal rotations around the N8-S7, N15-C4, and S7-C1 bonds, and inversions at two nitrogen atoms (N15 and N8). The four conformers can be divided into two groups: (a) *eclipsed* conformers (SAM_1 and SAM_3) and (b) *staggered* conformers (SAM_2 and SAM_4) which vary on the orientation of the *p*-amino group. These pairs of conformers SAM_1/SAM_3 and SAM_2/SAM_4 can be converted to each other by rotation about the N15-C4 or S7-C1 bonds as well as inversion at the N15 atom. Rotation about the N15-C4 bond requires activation energies larger than 30 kJ/mol while the S7-C1 bond needs to overcome barriers of about 10 to 15 kJ/mol, depending on the orientation of the *p*-amino group: for SAM_1/SAM_3 conversion, the transitional states contain a stabilizing interaction of the C-H $\cdots$ NH_2 type, which reduces the associated energy barrier. In SAM_2/SAM_4 conversion, the stabilizing interaction is replaced by C-H $\cdots$ H_2N repulsive interactions, leading to higher energy barriers. On the other hand, the energy barriers associated with the inversion of N15 are only about 1.5 kJ/mol.

These data allowed A. Borba *et al.*[12] to conclude that in the matrix isolation experiment, the higher energy conformer (SAM_3 and SAM_4) in each pair of structures (*staggered* or *eclipsed*) will undergo conformational relaxation to their most stable form (SAM_1 or SAM_2). Wherein, SAM_1 is rationalized by the presence of favourable interactions between the anti-parallel bond-

dipoles related with the N-H and S=O bonds while SAM_2 is stabilized by the H-bond type interaction of the NH ··· π nature but destabilized by the repulsion between the lone electron pairs of the oxygen atoms and N8. Overall, SAM_1 is the most stable conformer.

Rotation of N8-S7 bond and inversion of N8 atom allows the conversion of SAM_2 to SAM_1. According to the calculation of A. Borba *et al.*[12], the barrier rotation about the N8-S7 bond is ~14 kJ/mol (in the SAM_2 → SAM_1 direction) while the inversion at N8 atom is about 6 kJ/mol. Since the energy barrier for inversion of N8 atom is very low, it is expected to only see the most stable conformer (SAM_1) in the matrix due to conformational relaxation, which was eventually confirmed via FTIR experiment[12].

It will be interesting to analyse SAM using rotational spectroscopy to obtain its precise structural data and conformation. If He will be used as a carrier gas, conformational relaxation might be prevented. Thus, hopefully it will be possible to observe SAM_2 conformer in the spectrum.

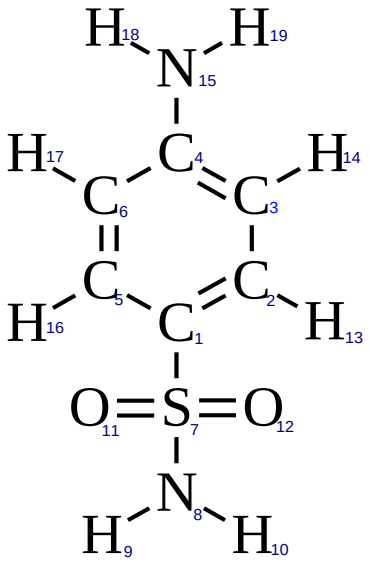

Figure 8.1 - Sketch of SAM showing the number of atoms used in the text.

Consequently, the structural parameters of SAM_1 (predicted global minimum) are presented in Table 8.2 while Figure 8.1 shows the numbering of the SAM atoms. This information is beneficial for the understanding of the mode of mechanism of the molecule.

Table 8.2 – Structural parameters calculated from the geometry MP2/6-311++G** of the global minimum (SAM_1).

Bond Length [Å]		Bond Angle [°]		Dihedral Angle [°]	
C2-C1	1.39859				
C3-C2	1.39346	<C3-C2-C1	119.325		
C4-C3	1.40715	<C4-C3-C2	120.799	<C4-C3-C2-C1	-1.280
C5-C1	1.39777	<C5-C1-C2	120.900	<C5-C1-C2-C3	0.900
C6-C5	1.39506	<C6-C5-C1	119.324	<C6-C5-C1-C2	-0.899
S7-C1	1.76761	<S7-C1-C2	119.457	<S7-C1-C2-C3	-178.262
N8-S7	1.68320	<N8-S7-C1	102.443	<N8-S7-C1-C2	83.547
H9-N8	1.01636	<H9-N8-S7	110.551	<H9-N8-S7-C1	101.286
H10-N8	1.01666	<H10-N8-S7	109.020	<H10-N8-S7-C1	-136.910
O11-S7	1.45553	<O11-S7-C1	107.446	<O11-S7-C1-C5	19.183
O12-S7	1.45442	<O12-S7-C1	108.480	<O12-S7-C1-C2	-27.758
H13-C2	1.08592	<H13-C2-C1	120.069	<H13-C2-C1-C5	-178.991
H14-C3	1.08782	<H14-C3-C2	119.662	<H14-C3-C2-C1	-179.773
N15-C4	1.39800	<N15-C4-C3	120.440	<N15-C4-C3-C2	177.009
H16-C5	1.08582	<H16-C5-C1	119.980	<H16-C5-C1-C2	-0.899
H17-C6	1.08781	<H17-C6-C5	119.648	<H17-C6-C5-C1	179.735
H18-N15	1.01135	<H18-N15-C4	114.520	<H18-N15-C4-C6	-27.196
H19-N15	1.01135	<H19-N15-C4	114.516	<H19-C13-C4-C3	27.421

NOTE: Numbering of SAM atoms is illustrated in Figure 8.1.

8.3 Substituent Effect

As can be seen in Figure 8.1, SAM is a substituted structure of BSA where -NH_2 group is added to the *para* position of the phenyl ring. Introduction of a substituent can modify the biological mechanism of a molecule through the alteration of the geometric and electronic properties. Hence, important structural parameters of BSA and SAM (obtained from Table 5.5 and Table 8.2 respectively) are compared in Table 8.3.

It can be observed that the addition of -NH_2 substituent resulted in the (1) slight decrease of the <O11-S7-C1 and <O11-S7-C1 angles and average S-C bond and (2) minimal lengthening of the N-S and O-S bonds and angles of <H9-N8-S7 and <O12-S7-C1, with respect to the corresponding parameters of unsubstituted BSA compound. Overall, the modifications are not significant. On the other hand, the HOMO energy is expected to increase since -NH_2 is a strong electron donating group.[48]

Table 8.3 – Selected geometric parameters of BSA and SAM from MP2/6-311++G** calculation and their calculated differences.

Parameter	BSA[a]	SAM	STRUCTURAL DIFFERENCE (BSA-SAM)
S7-C1 [Å]	1.77698	1.76761	0.00937
N8-S7 [Å]	1.67926	1.68320	-0.00394
O11-S7 [Å]	1.45376	1.45553	-0.00177
O12-S7 [Å]		1.45442	-0.00066
<H9-N8-S7 [º]	110.338	110.551	-0.213
<H10-N8-S7 [º]		109.020	1.318
<O11-S7-C1 [º]	107.616	107.446	0.17
<O12-S7-C1 [º]		108.480	-0.864
[a] – Original values before structural refinement			

From Table 8.3, it can be noticed that the optimized SAM (based on B3LYP and MP2 / 6-311++G**) is not symmetric. This is interesting because it is believed that sulfanilamide conformers belong to the C_s symmetry point group.[12] Thus, another frequency calculation with a constraint of symmetry was launched. The result showed a negative frequency which connotes that the symmetric conformation is a transition state and not the minimum. To check the result, a surface calculation (via B3LYP/6-311++G**) was performed. Wherein, the symmetric orientation was found to be a minimum. The derived data from the frequency and surface calculation clash to each other. For the above reasons, it would be very interesting to perform a rotational spectroscopy experiment in hope to better describe the symmetry and strange behaviour of SAM.

8.4 Conclusion

Four conformers of SAM were predicted using B3LYP and MP2 (at 6-311++G** level of theory) computational methods. Wherein, the global minimum exist in an eclipsed arrangement of the sulfonamide moiety and with the H atoms of the *p*-amino group pointed away on the other side of the phenyl ring. The preference for this conformation could be explained by the anti-parallel bond-dipole interactions between the N-H and S=O bonds. Moreover, SAM has a low barrier energy, associated either with internal rotations or inversions at the nitrogen atoms, which makes it susceptible to conformational relaxation. On the other hand, the *p*-amino substituent has no significant effects on the bond lengths and bond angles of BSA. Lastly, the optimized structure of SAM (via B3LYP and MP2 at 6-311++G** level) is not symmetric. The unusual conformation was verified by launching a surface calculation and frequency calculation

of a constraint symmetry. Result of the surface calculation showed that the symmetric conformation is a minimum but the frequency calculation says otherwise.

8.5 Recommendation

It will be interesting to study the rotational spectrum of SAM because it was never performed before and to check if the molecule really belongs to the C_s symmetry point group. Since the different conformations of SAM can interconvert through a low energy barrier, conformational relaxation will occur in the jet expansion. Thus, if He is used as a carrier gas, it might be possible to see the other conformers present because conformational relaxation will be prevented. Consequently, if the conformers of SAM have weak intensities then it is advisable to use a rotational spectrometer with a higher resolution.

Chapter 9 - Overall Conclusion

Rotational spectroscopy in free jet expansions coupled with high level theoretical calculations (B3LYP and MP2 at 6-311++G** level of theory) have been used to provide accurate information on the conformation, structure, dipole moment, and relative conformational energy of various sulfa-drugs (BSA, *p*-TSA, *o*-TSA, and SAM).

Based on the study conducted, the stabilization of the *eclipsed* over the *staggered* conformer occurs for all compounds. Rationalization behind this preference varies among the sulfa-drugs. For BSA, it is due to electrostatic interactions between O and H atoms of the sulfonamide group. Conversely, *p*-TSA is very similar from BSA but small differences such as presence of other stable conformers were seen. While for *o*-TSA, it is due to the attractive interaction between the methyl group and O-atom. Lastly, between the two possible *eclipsed* forms of SAM, the conformer that forms the anti-parallel bond dipole interaction wins. However, rotational spectroscopy experiment is still needed to be performed for SAM.

On the other hand, it can be noted *p*-TSA, *o*-TSA, and SAM molecules are substituted structures of BSA. Introduction of $-NH_2$ or $-CH_3$ groups (in *para* position) have no significant effects on the structural parameters of BSA while addition of $-CH_3$ group (in *ortho* position) brought some dramatic changes in terms of the bond angles.

Lastly, the experimentally derived V_3 energy barrier for the rotation of methyl group in o-TSA (around 6.081(5) kJ/mol) is in good agreement with the calculated B3LYP/6-311+G** barrier by V. Petrov *et al*[11] (around 5.858 kJ/mol) but much higher than the corresponding B3LYP calculated barrier for *p*-TSA (around 0.126 kJ/mol)[11]. The large differences in energy values can be an indication of the interaction between the methyl and the amino group. In *o*-TSA, rotation is hindered while there is almost free methyl rotation in *p*-TSA.

Chapter 10 – References

[1] K.E. Haneke. (2002). Chloramine-T [127-65-1] and Metabolite p-toluenesulfonamide [70-55-3]. Review of Toxicological Literature, Integrated Laboratory Systems, North Calorina. Retrieved from: http://ntp.niehs.nih.gov/ntp/htdocs/Chem_Background/ExSumPdf/ChloramineT_508.pdf]

[2] D. Richter, G. Massman, T. Taute, & U. Duennbier. (2009). Investigation of the fate of sulfonamides downgradient of a decommissioned sewage farm near Berlin, Germany. *J. Contam. Hydrol.* 106, 183-194. doi: 10.1016/j.jconhyd.2009.03.001

[3] D. Richter, U. Duennbier, G. Massmann, & A. Pekdeger. (2007). Quantitative determination of three sulfonamides in environmental water samples using liquid chromatography coupled to electrospray tandem mass spectrometry. *J. Chromatogr. A, 1557,* 115-121. doi: http://dx.doi.org/10.1016/j.chroma.2007.04.042

[4] S. Joshi, N. Khosla, D. Khare, & P. Tiwari. (2002). Synthesis and antibacterial screening of novel sulphonamide Mannich bases. *Acta Pharm,* 52, 197-206

[5] S.M. Zondhi, M. Johar, N. Singhal, S. G. Dastidar, R, Shukla, & R. Raghubir. (2000). Synthesis and anticancer, anti-inflammatory, and analgesic activity evaluation of some sulfa drug and acrifine derivatives. *Mon. Chem. 131*(5), 511-520

[6] J.J. Li, G.D. Anderson, E.G. Burton, J.N. Cogburn, J.T. Collins, D.J. Garland, S.A. Gregory, H.C. Huang, P.C. Isakson, C.M. Koboldt, E.W. Logusch, M.B. Norton, W.E. Perkins, E.J. Reinhard, K. Seibert, A.W. Veenhuizen, Y. Zhang, & D.B. Reitz. 1,2-Diarylcyclopentenes as selective cyclooxygenase-2 inhibitors and orally active anti-inflammatory agents. (1995). *J. Med. Chem. 38*(22), 4570-8

[7] C.T. Supuran, A. Scozzafava, & A. Casini. (2003). Carbonic anhydrase inhibitors. *Med. Res. Rev. 23*(2), 146-89

[8] A. Ajibola, P. Gago-Ferrero, P.L. Borova, M.E. Dasenaki, A.A. Bletsou, & N.S. Thomaidis. (2015). Benzosulfonamides in wastewater: Method development, occurrence, and removal efficiencies. *Chemosphere. 119,* S21-S27. doi: http://dx.doi.org/10.1016/j.chemosphere.2014.04.003

[9] S. Melandri, S. Ragno, & A. Maris. (2009). Shape of Biomolecules by Free Jet Microwave Spectroscopy: 2-Amino-1-phenylethanol and 2-Methylamino-1-phenylethanol. *J. Phys. Chem,. A. 113,* 7769-7773

[10] V. Petrov, V. Petrova, G.V. Girichev, H. Oberhammer, N.I. Giricheva, & S. Ivanov. (2006). Molecular Structure and Conformations of Benzenesulfonamide: Gas Electron Diffraction and Quantum Chemical calculations. *J. Org. Che. 71,* 2952-2956

[11] V.M. Petrov, G.V. Girichev, H. Oberhammer, V.N. Petrova, N.I. Giricheva, A.V. Bardina, & S.N. Ivanov. (2008). Molecular Structure and Conformations of *para*-Methlybenzene Sulfonamide and *ortho*-Methylbenzene Sulfonamide: Gas Electron Diffraction and Quantum

Chemical Calculations Study. *J. Phys. Chem., 112*, 2969-2976. doi: http://dx.doi.org/10.1021/jp710532z

[12] A. Borba, A. Gomez-Zavaglia, & R. Fausto. (2013). Conformational Landscape, Photochemistry, and Infrared Spectra of Sulfanilamide. *J. Phys. Chem. 117*, 704-717. doi: http://dx.doi.org/10.1021/jp311789fl

[13] W.M. Haynes. (2013). *CRC Handbook of Chemistry and Physics, 94th Edition*. CRC Press, FL

[14] R. Naaman & Z. Vager. (2012). *The Structure of Small Molecules and Ions*. Plenum Press, NY

[15] C.H. Townes & A.L. Shawlow. (1955). *Microwave Spectroscopy*. McGraw-Hill Book Co., NY

[16] W. Gordy, W.V. Smith, & R.F. Trambarulo. (1953). *Microwave Spectroscopy*. John Wiley & Sons, Inc. NY

[17] P. Atkins & J. de Paula. (2006). *Atkins' Physical Chemistry* (8th Edition). New York, NY: Oxford University Press

[18] P.F. Benrath. (2000). *Molecular Spectroscopy and Structur*e, *in A Physicist's Desk Reference, Third Edition*, E.A. Cohen, D.R. Lide, & G. Trigg, eds., AIP Press

[19] J.K.G. Watson. (1977). *Vibrational Spectra and Structure*. Elsevier, Amsterdam

[20] G.W. King, R.M. Hainer, & P.C. Cross. (1943). The Asymmetric Rotor. I. Calculation and Symmetry Classification of Energy Levels. *J. Chem. Phys. 11*, 27

[21] B.S. Ray. (1932). *Z. Physik. 78*, 74

[22] G. Herzberg. (1945). *Structure and Molecular Spectra, Vol. II. Infrared and Raman Spectra of Polyatomic Molecules.* D. Van Nostrand Company, Inc. NY

[23] Z. Kisiel. PROSPE – Programs for ROtational SPEctroscopy. URL: http://info.ipfan.edu.pl/~kisiel/prospe.htm

[24] M. J. Frisch, G. W. Trucks, H. B. Schlegel, G. E. Scuseria, M. A. Robb, J. R. Cheeseman, G. Scalmani, V. Barone, B. Mennucci, G. A. Petersson, H. Nakatsuji, M. Caricato, X. Li, H. P. Hratchian, A. F. Izmaylov, J. Bloino, G. Zheng, J. L. Sonnenberg, M. Hada, M. Ehara, K. Toyota, R. Fukuda, J. Hasegawa, M. Ishida, T. Nakajima, Y. Honda, O. Kitao, H. Nakai, T. Vreven, J. A. Montgomery, Jr., J. E. Peralta, F. Ogliaro, M. Bearpark, J. J. Heyd, E. Brothers, K. N. Kudin, V. N. Staroverov, T. Keith, R. Kobayashi, J. Normand, K. Raghavachari, A. Rendell, J. C. Burant, S. S. Iyengar, J. Tomasi, M. Cossi, N. Rega, J. M. Millam, M. Klene, J. E. Knox, J. B. Cross, V. Bakken, C. Adamo, J. Jaramillo, R. Gomperts, R. E. Stratmann, O. Yazyev, A. J. Austin, R. Cammi, C. Pomelli, J. W. Ochterski, R. L. Martin, K. Morokuma, V. G. Zakrzewski, G. A. Voth, P. Salvador, J. J. Dannenberg, S. Dapprich, A. D. Daniels, O. Farkas, J. B. Foresman, J. V. Ortiz, J. Cioslowski, & D. J. Fox. 2013. *Gaussian 09, Revision D.01*. Gaussian, Inc., Wallingford CT

[25] D.A. McQuarrie & J.D. Simon. (1997). *Physical Chemistry: A Molecular Approach*. University Science Books, CA

[26] P. Hohenberg & W. Kohn. (1964). Inhomogeneous Electron Gas. *Phys. Rev. 136,* B864]; [W. Kohn & L.J. Sham. (1965). Self Consistent Equations Including Exchange and Correlation Effects. *Phys. Rev. 140,* A1133

[27] R.G. Parr & W. Young. (1989). *Density-Functional Theory of Atoms and Molecules*. Oxford University Press, New York

[28] J. Almlöf & T. Helgaker. (1988). Gaussian Basis Sets for High-Quality ab Initio Calculations. *J. Phys. Chem. 92*, 3029-3033

[29] J. Laane. (2011). *Frontiers of Molecular Spectroscopy*. Elsevier, Netherlands

[30] T. Imasaka, D.S. Moore, & T. Vo-Dinh. (2003). Critical assessment: Use of supersonic jet spectrometry for complex mixture analysis (IUPAC Technical Report). *Pure Appl. Chem., 75*(7), 975-998

[31] S.-Y. Tang, Z.-N. Xia, Y.-J. Fu, & Q. Gou. (2008) *Chin.* J. Advances and Applications of Microwave Spectroscopy. *Chin. J. Anal. Chem. 36,* 1145-1151

[32] M.V. Johnston. (1984). Supersonic jet expansions in analytical spectroscopy. *TrAC. 3*(2), 58-61. doi: http://dx.doi.org/10.1016/0165-9936(84)87055-7

[33] R.D. Brown, J.G. Crofts, P.D. Godfrey, D. McNaughton, & A.P. Pierlot. (1988). A stark-modulated supersonic nozzle spectrometer for millimetre-wave spectroscopy of larger molecules of low volatility. *J. Mol. Struct., 190,* 185-193. doi: http://dx.doi.org/10.1016/0022-2860(88)80283-7

[34] S. Melandri, W. Caminati, L.B. Favero, A. Millemaggi, & P.G. Favero. (1995). A microwave free jet absorption spectrometer and its first application. *J. Mol. Struct., 352/353,* 253-258

[35] S. Melandri, G. Maccaferri, A. Maris, A. Millemaggi, W. Caminato, & P.G. Favero. (1996). Observation of the rotational spectra of van der Waals complexes by free jet absorption millimetre wave spectroscopy: pyridine-argon. *Chem. Phys. Lett. 261,* 267-271

[36] Z. Kisiel. (2001). *In: J. Demaison et al. (Eds.), Spectroscopy from Space,* Kluwer Academic Publishers, 91-106

[37] I.I. Ioannou & R.L. Kuczkowski. (1994). The Microwave Spectrum and Structure of the Argon-Acetaldehyde van der Waals Complex. *J. Mol. Spectrosc.* 166, 354-364

[38] R. Fausto (ed.). (1996). *Low Temperature Molecular Spectroscopy*. Kluwer Academic Publishers, The Netherlands

[39] H. Haken & H.C. Wolf. (2013). *Molecular Physics and Elements of Quantum Chemistry: Introduction to Experiments and Theory*. Springer-Verlag Berlin Heidelberg, New York

[40] R.S. Ruoff, T.D. Klots, T. Emilson, & H.S. Gutowski. (1990). Relaxation of conformers and isomers in seeded supersonic jets of inert gases. *J. Chem. Phys., 93*, 129. doi: http://dx.doi.org/10.1063/1.458848

[41] R.S. Ruoff, T.D. Klots, T. Emilsson, & H.S. Gutowsky. (1990). Rotational spectra and structures of small clusters containing the hydrogen cyanide dimer: X-(HCN)2 with X = carbon monoxide, molecular nitrogen, ammonia, and water. *J. Chem. Phys.*, *93*, 6363-70

[42] J. Kraitchman. (1953). Determination of molecular structure from microwave spectroscopic data. *Am. J. Phys.21*, 17-24

[43] B.M. Giuliano, P. Ottaviani, L.B. Favero, & W. Caminati. (2007). Conformational preferences of chiral molecules: free jet rotational spectrum of 1-phenyl-1-propanol. *Phys. Chem. Chem. Phys., 9*, 4460-4464. doi: http://dx.doi.org/10.1039/b705114J

[44] N.I. Giricheva, G.V. Girichev, M.S. Fedorov, & S.N. Ivanov. (2013). Substituent effect on geometric and electronic structure of benzenesulfonic acid: gas-phase electron diffraction and quantum chemical studies of 4-CH3C6H4SO3H and 3-NO2C6H4SO3H. *Struct Chem*. *24*, 807-818. doi: 10/1007/s11224-01300238-9

[45] C. Calabrese, A. Maris, L. Evangelisti, W. Caminati, & S. Melandri. (2013). Fluorine Substitution Effects on Flexibility and Tunneling Pathways: The Rotational Spectrum of 2-Fluorobenzylamine. *ChemPhysChem. 14*, 1943-1950. doi: http://dx.doi.org/10.1002/cphc.201300121

[46] H. Hartwig & H. Dreizler. (1996). The Microwave spectrum of trans-2,3-Dimethyloxirane in Torsional Excited States. *Z. Naturforsch*. *51a*, 923-932

[47] F.A. Carey & R.J. Sundberg. (1990). Advanced Organic Chemistry: Part A: Structure and Mechanisms (3rd Edition). Plenum Press, New York

[48] F. Fringuelli & A. Taticchi. (2002). The Diels-Alder Reaction: Selected Practical Methods. John Wiley & Sons, New York